Fiber-Specific Structural Properties Relate to Reading Skills in Children

Steven Lee Meisler[1,2*] **and John D.E. Gabrieli**[2,3]

***For correspondence:**
smeisler@g.harvard.edu (SLM)

Present address:
Department of Brain & Cognitive Sciences, Massachusetts Institute of Technology, 43 Vassar Street, Cambridge, MA 02139, USA

[1]Program in Speech and Hearing Bioscience and Technology, Harvard Medical School, 260 Longwood Avenue, Boston, MA 02115, USA; [2]Department of Brain & Cognitive Sciences, Massachusetts Institute of Technology, 43 Vassar Street, Cambridge, MA 02139, USA; [3]McGovern Institute for Brain Research, 43 Vassar Street, Cambridge, MA, 02139 USA

Abstract

Recent studies suggest that the cross-sectional relationship between reading skills and white matter microstructure, as indexed by fractional anisotropy, is not as robust as previously thought. Fixel-based analyses yield fiber-specific micro- and macrostructural measures, overcoming several shortcomings of traditional DTI approaches. We ran a whole-brain analysis investigating whether fixel-derived metrics related to single-word reading skills in a large, open, quality-controlled data set of 983 children and adolescents ages 6-18. We also compared fixel metrics between participants with (*n* = 102) and without (*n* = 570) reading disabilities. We found that the product of fiber density (FD) and cross-section (FC), or FDC, positively related to reading skills throughout the brain, especially in left temporoparietal and cerebellar white matter, but did not differ between groups. Exploratory analyses revealed that among metrics from other diffusion models - DTI, DKI, and NODDI - only orientation dispersion index (ODI) from NODDI was associated (inversely) with reading skills. Our findings further support the importance of left-hemisphere dorsal temporoparietal white matter tracts in reading. Additionally, our results suggest future DWI studies of reading should be designed to benefit from advanced diffusion models, include cerebellar coverage, and consider continuous analyses that account for individual differences in reading skill.

Introduction

Many research efforts spanning multiple neuroimaging modalities have sought to yield insights into the neural bases of reading ability and disability (***Vandermosten et al., 2012***; ***Landi et al., 2013***; ***Richlan et al., 2013***). Among these studies are those that employ diffusion-weighted imaging (DWI) to study properties of anatomical connections in the brain. The most commonly reported measure of white matter microstructure is fractional anisotropy (FA). FA is a metric derived from the diffusion tensor imaging (DTI) model (***Basser et al., 1994***) that quantifies the degree to which water diffusion is directionally dependent in each voxel (***Hagmann et al., 2006***; ***Basser and Pierpaoli, 1996***). FA is high in white matter compared to gray matter and cerebrospinal fluid (CSF) due to preferential water movement along the axis of axons. Studies of white-matter microstructural properties' relationships to reading have primarily employed FA (for overviews, see ***Ben-Shachar et al.*** (***2007***); ***Vandermosten et al.*** (***2012***); ***Moreau et al.*** (***2018***); ***Meisler and Gabrieli*** (***2022***)). However, several factors confound the ability to draw meaningful interpretations from FA results (***Farquharson et al., 2013***; ***Riffert et al., 2014***). As a metric defined on the voxel-level, FA is prone to partial volume effects, manifesting as reduced FA in regions where white matter borders gray matter or CSF (***Vos et al., 2011***). Due to the limited degrees-of-freedom in the tensor model, FA is artificially lower in regions of crossing fibers, affecting up to 90% of white matter voxels (***Behrens et al., 2007***; ***Jeurissen et al., 2013***). In addition to sensitivity to myelination, FA also tends to covary with other elements such as axonal diameter, density, permeability, and coherence (***Beaulieu, 2009***; ***Johansen-Berg and Behrens, 2013***; ***Shemesh, 2018***; ***Friedrich et al., 2020***; ***Lazari and Lipp, 2021***), and information from DTI alone is not sufficient to gauge the individual contributions of these features. Thus, FA has often been reduced to a nonspecific (and arguably inappropriate; see ***Jones et al.*** (***2013***)) term, "white matter integrity."

Early cross-sectional studies of FA and reading skills seemed to converge towards a consensus of greater FA relating to better reading ability, particularly in left temporoparietal white matter tracts that connect neocortical regions known to be important for language, such as the arcuate fasciculus (AF) and superior longitudinal fasciculus (SLF) (***Klingberg et al., 2000***; ***Ben-Shachar et al., 2007***; ***Vandermosten et al., 2012***). As tract segmentation algorithms became more robust and widely used, subsequent studies, empowered to address tract-specific hypotheses, began describing previously unreported results. These included significant FA-reading relationships in different areas, such as commissural (***Frye et al., 2008***; ***Lebel et al., 2013***), cerebellar (***Travis et al., 2015***; ***Bruckert et al., 2020***), and right-lateralized bundles (***Horowitz-Kraus et al., 2015***), as well as regions where higher FA was associated with worse reading skills (***Carter et al., 2009***; ***Frye et al., 2011***; ***Christodoulou et al., 2017***). The inconsistency in past results are potentially driven by a variety of factors such as publication bias (***Begg, 1994***), small participant cohorts, inhomogeneous acquisition parameters, different covariates and reading measures, variation in age groups, and different processing techniques (***Moreau et al., 2018***; ***Ramus et al., 2018***; ***Schilling et al., 2021a***,b). Few studies have sought to resolve these inconclusive results. A meta-analysis of whole-brain voxel-based studies found no regions where FA either varied with reading ability or was reduced in dyslexic, compared to typically reading, individuals (***Moreau et al., 2018***). ***Geeraert et al.*** (***2020***) used principal

component analysis to draw out white matter structural indices from several scalar maps, including metrics from DTI (such as FA) and neurite orientation dispersion and density imaging (NODDI; ***Zhang et al.*** (***2012***)), and found that variance in these measures were driven by age-related development, but not reading. Three large-scale cross-sectional studies using publicly available data sets found largely null associations between FA and reading skills in several tracts (***Koirala et al., 2021***; ***Meisler and Gabrieli, 2022***; ***Roy et al., 2022***).

Despite the mixed empirical findings relating FA to variation in reading ability, it is reasonable to hypothesize that there ought to be such a brain structure-behavior correlate of reading ability. Reading involves the functioning of a widely distributed brain network (***Cattinelli et al., 2013***; ***Wandell and Yeatman, 2013***; ***Murphy et al., 2019***), and white matter tracts are conduits for information sent within this network (***Ben-Shachar et al., 2007***). Lesion-mapping analyses (***Wang et al., 2020***; ***Li et al., 2021***) and clinical case studies (***Epelbaum et al., 2008***; ***Rauschecker et al., 2009***) have demonstrated that white matter connections, primarily in the left hemisphere, are necessary for reading. Since myelin is a plastic structure that is shaped by learning and can modulate neuronal firing patterns (***Fields, 2015***; ***Xin and Chan, 2020***), it is reasonable to suspect that functional variation, such as differences in reading ability, may be reflected by *some* white matter structural property (***Ramus et al., 2018***; ***Protopapas and Parrila, 2018***, ***2019***). The largely null findings in higher-powered meta-analyses (***Moreau et al., 2018***) and large-scale studies (***Koirala et al., 2021***; ***Meisler and Gabrieli, 2022***; ***Roy et al., 2022***) suggest that FA is not a specific enough metric to effectively capture this relationship in cross-sectional designs.

More advanced diffusion models have yielded metrics that better reflect variance in reading skills. ***Sihvonen et al.*** (***2021***) found that connectometry from quantitative anisotropy modeling (***Yeh et al., 2013***) in multiple pathways covaried with better reading skill independently from phonological abilities. Quantitative anisotropy is less prone to artifacts from partial volume effects and crossing fibers (***Yeh et al., 2016***). ***Koirala et al.*** (***2021***) employed multiple diffusion models in children and concluded that lower orientation dispersion and neurite density indices from NODDI modeling related to better reading abilities in several bilateral tracts, while FA was not associated with reading. Although not a DWI sequence, myelin water imaging (MWI) studies have suggested both positive (***Beaulieu et al., 2020***) and negative (***Economou et al., 2022***) associations of myelination with reading skill in children. ***Economou et al.*** (***2022***) also replicated null associations between FA and reading in their experimental cohort. These results collectively suggest that studies of reading (and perhaps other cognitive domains, see ***Lazari et al.*** (***2021***)) should begin to move beyond traditional DTI modeling. However, NODDI metrics, being a voxel-level metric, cannot ascribe properties to particular fiber populations if multiple exist in a voxel. MWI acquisitions, while showing high specificity to variation in myelin, tend to have relatively long scan times (***Alonso-Ortiz et al., 2015***); one would also still need to collect a DWI scan if one wanted to associate MWI metrics with fiber bundles and properly account for MWI variation due to fiber orientations (***Birkl et al., 2021***). Collecting all of these data in children and clinical populations is challenging and not always practical.

Subsequently, a DWI analytical paradigm was introduced that performs statistical in-

ferences on "fixels," or individual fiber populations within voxels, using a set of three fixel-derived metrics: fiber density (FD), fiber cross-section (FC), and their product (FDC) (***Raffelt et al., 2015***, ***2017b***). This framework is enabled by constrained spherical deconvolution (CSD) (***Tournier et al., 2007***), a data-driven approach for resolving fiber orientation distributions (FODs) in the presence of crossing fibers. Unlike other fiber-specific metrics, such as quantitative anisotropy, fixel-based analyses can yield distinct micro- and macrostructural components. FD is a microstructural measure that reflects the intra-axonal volume fraction (***Raffelt et al., 2012b***; ***Genc et al., 2020***), while FC is a macrostructural measure related to the cross-sectional area of fiber bundles (***Raffelt et al., 2017b***). The product of FD and FC, or FDC, is therefore related to the total estimated intra-axonal volume and is sensitive to both white matter micro- and macrostructure. FDC is thought to reflect the capacity of white matter to relay information (***Raffelt et al., 2017b***).

In addition to enabling investigations of these more specific fixel-derived metrics, fixel-based analyses (FBA) present several additional advantages compared to traditional FA whole-brain approaches (***Dhollander et al., 2021b***). Since FBAs operate on the level of fixels, and fixels are generated from FODs in white matter, FBAs are by nature restricted to white matter, thus mitigating effects of multiple comparison correction from redundant regions that often undermine whole brain voxel-based analyses. Spatial smoothing in FBAs is performed within local neighborhoods of white matter bundles informed by fixel connectivity (***Raffelt et al., 2015***). Thus, the signal in a given fixel is not influenced by different tissue classes or other fiber populations, in contrast to traditional voxel-based spatial smoothing which operates more indiscriminately.

FBAs have been quickly adopted and used to investigate several clinical and developmental populations (reviewed in ***Dhollander et al.*** (***2021b***)). However, they have not yet been used to examine reading abilities. With the increased specificity of FBAs, this approach might reveal fiber-specific biomarkers that are more sensitive to variation in reading abilities than FA or other tensor-derived metrics, providing valuable insights into the neural basis of literacy. In this study (Figure 1), we examined the relationship between fixel metrics and single-word reading skill in a pediatric data set of 983 children ages 6-18 from the Healthy Brain Network biobank (***Alexander et al., 2017***). We additionally looked for differences in fixel metrics between participants with (n = 102) and without reading disabilities (n = 570), using criteria based on diagnostic and standardized cognitive assessments. We employed generalized additive modeling (GAM) (***Hastie and Tibshirani, 1990***) to more flexibly model age-related variance given the wide age range of participants (***Zhao et al., 2022***; ***Bethlehem et al., 2022***). Based on findings from NODDI (***Koirala et al., 2021***), quantitative anisotropy (***Sihvonen et al., 2021***), and MWI (***Beaulieu et al., 2020***; ***Economou et al., 2022***) studies, we hypothesized that we would see positive associations between fixel-metrics and reading abilities in several tracts spanning both hemispheres, but especially the left arcuate fasciculus, left inferior fronto-occipital fasciculus, and cerebellar peduncles, as these tracts yielded significant relationships in multiple studies of advanced diffusion models and reading. However, since this was the first FBA involving reading skill, and one with considerably high statistical power, we took a more conservative approach and ran a whole-brain FBA. Using tract segmentation, we ascribed locations of significant results to bundles to guide future research efforts.

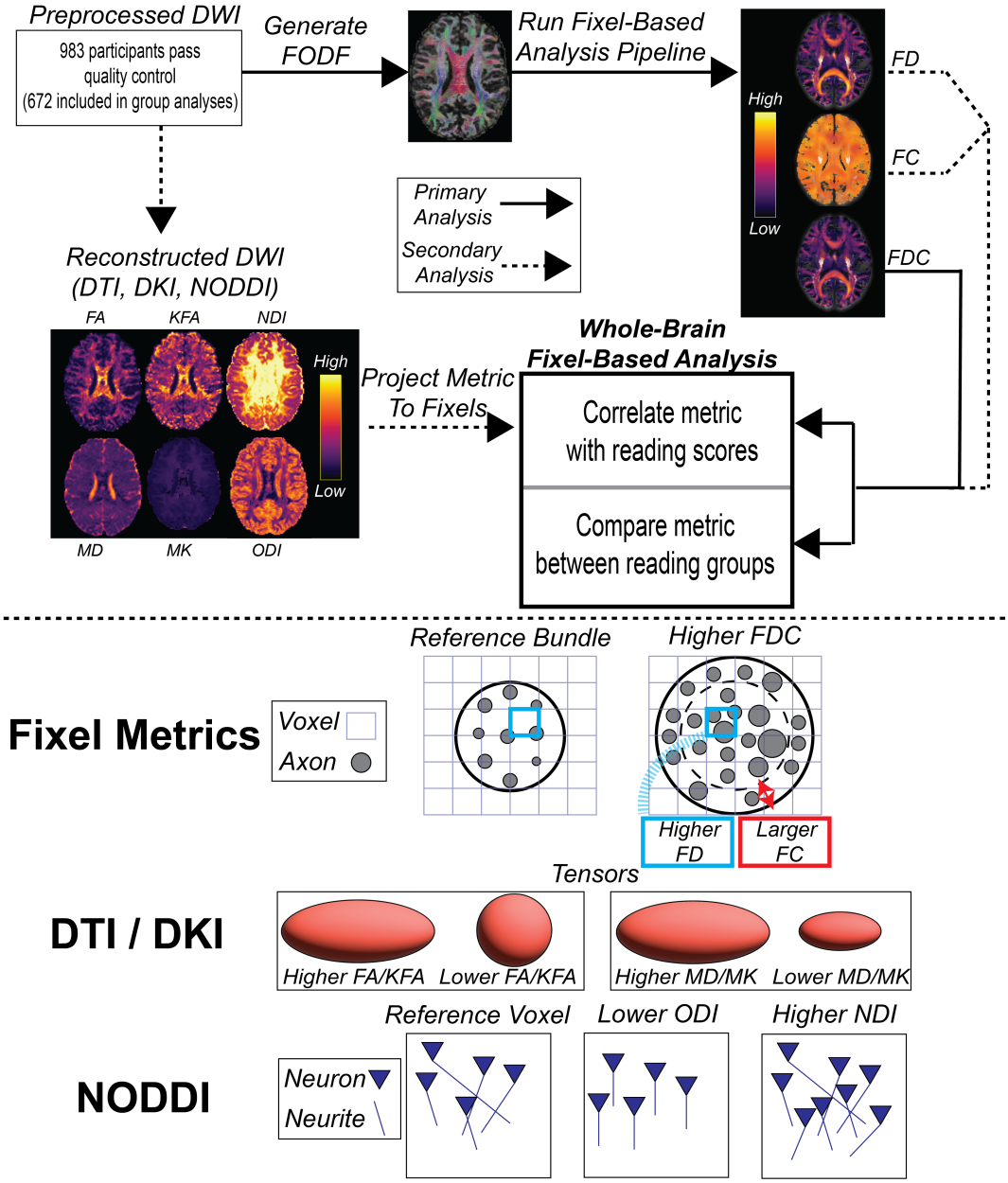

Figure 1. *Top*: Methodological overview of the paper, including both primary and secondary analyses. *Bottom*: Schematic depicting interpretations of changes in examined metrics. Depictions of bundles, axons, and neurites are not drawn to scale. *Abbreviations*: DWI - diffusion weighted imaging; DTI - diffusion tensor imaging; DKI - diffusion kurtosis imaging; NODDI - neurite orientation density and dispersion index; FA - fractional anisotropy; KFA - kurtosis fractional anisotropy; MD - mean diffusivity; MK - mean kurtosis; NDI - neurite density index; ODI - orientation dispersion index; FODF - fiber orientation distribution function; FD - fiber density; FC - fiber cross-section; FDC - fiber density and cross-section product.

Results

Participant Data

The 983 participants who passed all inclusion, exclusion, and quality control criteria (Table 1) were divided into a Typically Reading (TR; n = 570) and Reading Disability group (RD; n = 102) based on diagnostic and standardized cognitive assessments (Figure 2; see *Methods and Materials*). 311 participants did not meet the criteria for either group, but were still included in the correlation analyses. The TR group, compared to the RD group, was older and had higher socioeconomic scores, brain volumes, verbal IQ, visuospatial IQ, reading scores, globally-averaged fixel metrics, and image quality (as indexed by the average neighbor correlation; see ***Yeh et al.*** (***2019***) for more information on this metric). The groups were matched in sex distribution (although the cohort as a whole was male-skewed), handedness, and average motion (mean framewise displacement). Reading scores and IQs were age-standardized composite indexes from the Tests of Word Reading Efficiency (TOWRE; ***Torgesen et al.*** (***1999***)) and Wechsler Intelligence Scale for Children (WISC; ***Wechsler and Kodama*** (***1949***)), respectively. 17 participants were missing socioeconomic information, and 93 participants did not have WISC scores. Since these variables were not ultimately included in our statistical models, we did not exclude these participants. Relationships between phenotypic and neuroimaging metrics, and differences in these measures between sites, can be found in the supplementary materials (Table S1; Figures S1 and S2).

Metric	All	TR	RD	Effect Size
n	983	570	102	-
Sex [M / F]	617 / 366	355 / 215	59 / 43	ϕ = 0.0235
Age [years]	11.16 (0.10)	11.38 (0.14)	10.56 (0.27)	d = 0.258*
Handedness [EHI]	61.78 (1.58)	62.19 (2.05)	62.91 (5.05)	d = 0.015
Handedness [L/A/R]	74 / 128 / 781	42 / 66 / 462	8 / 17 / 77	ϕ = 0.047
SES [Yrs. Parental Edu.]	17.63 (0.10)	18.13 (0.11)	16.93 (0.32)	d = 0.429†
ICV [cm^3]	1540 (5.130)	1559 (6.735)	1501 (12.47)	d = 0.370†
WISC VSI	102.08 (0.552)	105.72 (0.714)	97.82 (1.497)	d = 0.494†
WISC VCI	104.61 (0.542)	109.26 (0.658)	98.18 (1.414)	d = 0.750†
TOWRE	97.93 (0.56)	109.49 (0.45)	70.48 (0.80)	d = 3.74†
Global FD	0.285 (6.26e-4)	0.287 (7.66e-4)	0.280 (2.53e-3)	d = 0.337*
Global log(FC)	0.050 (2.15e-3)	0.059 (2.73e-3)	0.030 (5.92e-3)	d = 0.455†
Mean Motion	0.44 (7.89e-3)	0.44 (0.01)	0.44 (0.03)	d = 4.27e-3
Quality [Neighbor Corr.]	0.756 (1.58e-3)	0.760 (2.08e-3)	0.745 (5.17e-3)	d = 0.291*

Table 1. Phenotypic and neuroimaging summary statistics in all participants and within the two reading proficiency groups. 17 and 93 participants were lacking socioeconomic and WISC scores, respectively, and were ignored for the corresponding rows. Values are listed as mean (standard error of the mean). For group comparison effect sizes (right-most column), * denotes $p < 0.05$ and † denotes $p < 0.001$. All t-tests were Welch's t-tests. *Abbreviations*: TR - typically reading group; RD - reading disability group; EHI - Edinburgh Handedness Inventory; SES - socioeconomic status; ICV - intracranial volume; TOWRE - Tests of Word Reading Efficiency composite score, age-normalized; WISC VSI - Wechsler Intelligence Scale for Children visuospatial index, age-normalized; WISC VCI - Wechsler Intelligence Scale for Children verbal comprehension index, age-normalized; FD - Fiber density; FC - fiber cross-section. FD and FC are unit-less.

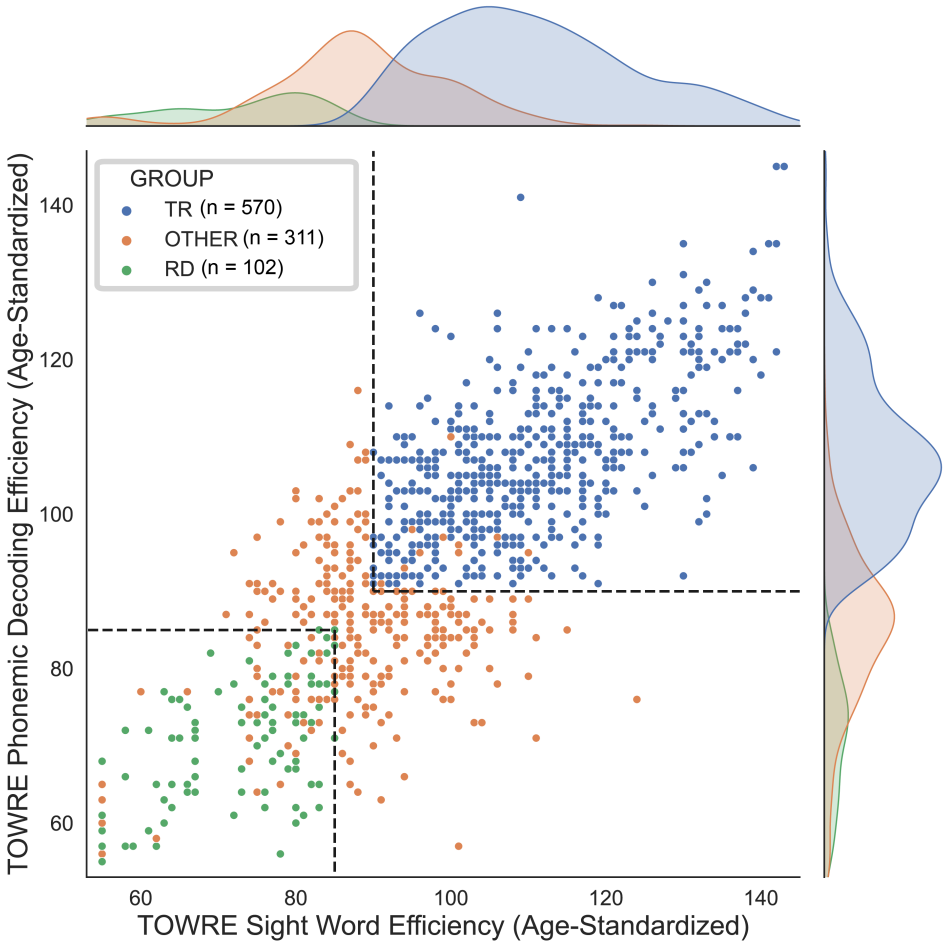

Figure 2. Age-standardized TOWRE sub-scores of all participants. Each dot represents a participant, color-coded by group assignment. Dashed lines mark the score cut-offs for the two reading proficiency groups. Since scores are discrete and not unique, some dots may overlap with each other. Kernel density estimation plots along the perimeter show the distribution of reading scores in each group. *Abbreviations*: TR - typically reading group; RD - reading disability group; TOWRE - Tests of Word Reading Efficiency.

Continuous Analyses

We ran a whole-brain fixel-based analysis testing whether the product of fiber density and fiber cross-section, or FDC, was associated with reading skills. We found widespread bilateral and commissural regions in which higher FDC was significantly related to better reading abilities ($q_{FDR} < 0.05$; Figure 3). Each tract produced by the segmentation software, *TractSeg* (***Wasserthal et al., 2018a***), contained significant fixels (Table 2). We defined effect size in each fixel as the difference in adjusted R^2 values between the full model and a reduced model without the predictor of interest (TOWRE scores or group designations). The effect size of significant fixels varied up to a peak value of 0.034. Clusters of fixels with the largest effect sizes ($\Delta R^2_{adj} > 0.03$) were observed in left-hemisphere temporoparietal and cerebellar white matter. Tract segmentation intersections (Table 2) revealed that the temporoparietal cluster was most likely associated with the left arcuate fasciculus (AF), superior longitudinal fasciculus (SLF), or middle longitudinal fasciculus (MLF). These tracts largely overlapped (Figure S3). The cerebellar cluster was most likely associated with the left superior cerebellar peduncle (SCP). Homotopic clusters of significant fixels were observed in right-hemisphere temporoparietal and cerebellar white matter, but they reached smaller effect sizes than those in the left hemisphere. See the supplementary material for significant fixels colored by direction and beta values (Figure S4). *Post-hoc* exploration of FD and FC revealed diffuse associations of better reading skills with higher FC, as compared to fewer regions where higher FD was related to better reading (Figure S5). As expected, highest effect sizes of FDC were achieved in regions where FD and FC were both independently related with better reading.

Group Analyses

We did not find any significant differences in FDC between the TR and RD groups. *Post-hoc* exploration further revealed no differences in FD between the groups, but did yield regions where the TR group had higher FC in bilateral cerebellar tracts, bilateral anterior temporal lobe, and left fronto-parietal white matter (Figure S6).

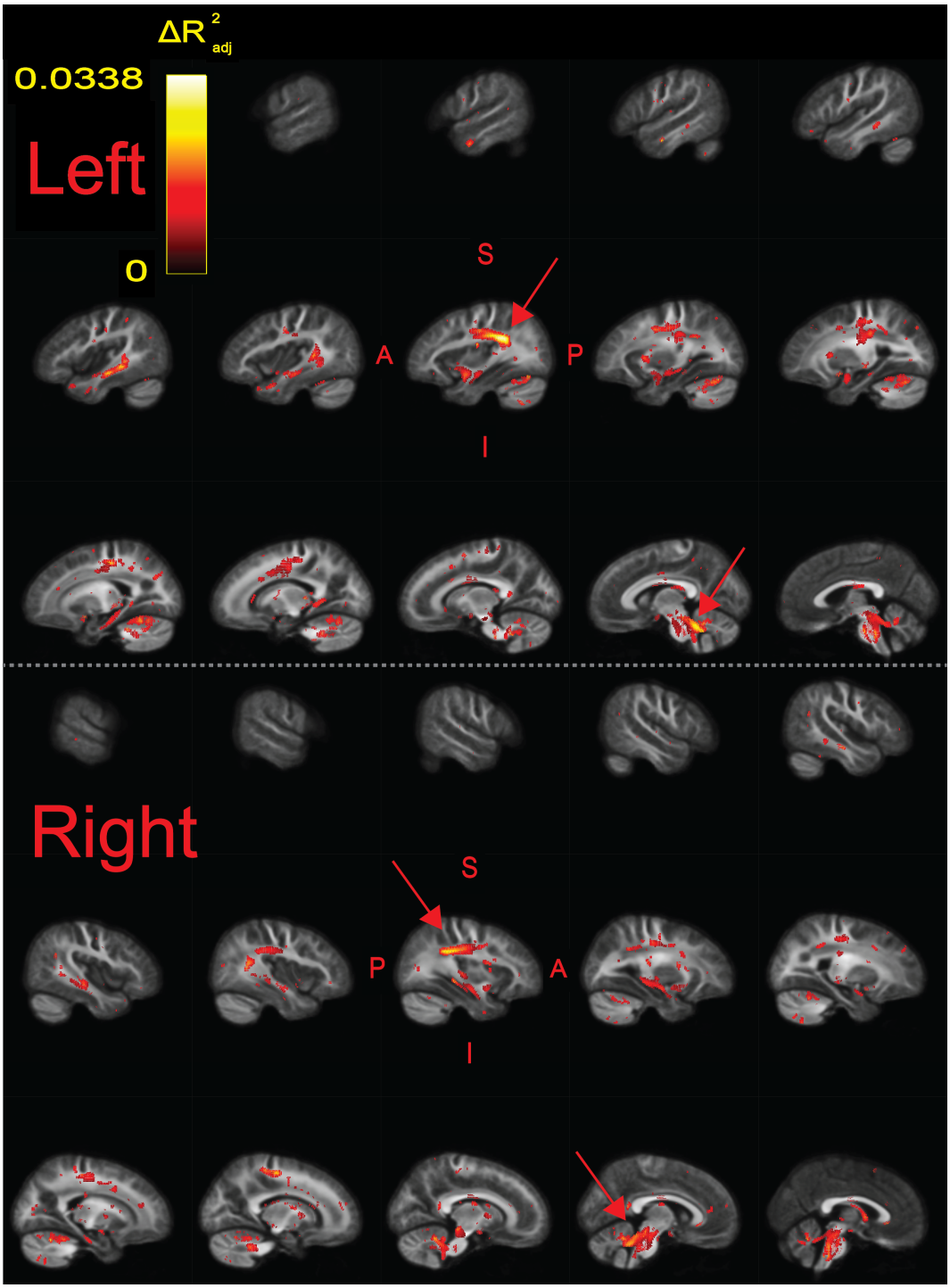

Figure 3. Significant fixels ($q_{FDR} < 0.05$) for relating FDC to TOWRE scores, colored by effect size (ΔR^2_{adj}). Model confounds included a spline fit for age and linear fits for sex, site, neighbor correlation, and log(ICV). Top and bottom panels are left and right hemispheres, respectively. Sagittal slices go from lateral-to-medial. Red arrows point to larger clusters of fixels in bilateral temporoparietal and cerebellar white matter that were associated with higher effect sizes relative to fixels in the rest of the hemisphere. The template FOD image was used as the background image.

Tract	N Fixels ($q_{FDR} < 0.05$)	N Fixels ($q_{FDR} < 0.001$)	Max Effect Size (ΔR^2_{adj})
AF	2705 / 1814	382 / 130	0.032 / 0.024
ATR	88 / 309	0 / 0	0.018 / 0.015
CA	337	0	0.0005
CC_1	81	0	0.018
CC_2	1614	0	0.018
CC_3	286	0	0.013
CC_4	1532	0	0.020
CC_5	1132	0	0.014
CC_6	1819	73	0.025
CC_7	219	0	0.018
CG	373 / 270	0 / 0	0.018 / 0.018
CST	2113 / 1543	125 / 146	0.023 / 0.0.22
FPT	3010 / 2788	342 / 358	0.026 / 0.025
FX	328 / 263	10 / 10	0.024 / 0.024
ICP	913 / 691	19 / 41	0.026 / 0.022
IFOF	1164 / 780	55 / 0	0.024 / 0.018
ILF	867 / 302	53 / 3	0.023 / 0.022
MCP	2389	39	0.022
MLF	1661 / 623	185 / 28	0.032 / 0.001
OR	547 / 356	26 / 0	0.023 / 0.017
POPT	2264 / 1820	187 / 188	0.025 / 0.022
SCP	1585 / 1385	192 / 156	0.034 / 0.022
SLF I	901 / 1293	38 / 81	0.021 / 0.022
SLF II	1150 / 1470	141 / 136	0.031 / 0.024
SLF III	846 / 604	222 / 57	0.032 / 0.024
ST_FO	141 / 120	0 / 0	0.018 / 0.014
ST_OCC	845 / 610	51 / 0	0.024 / 0.017
ST_PAR	1458 / 1057	27 / 66	0.024 / 0.024
ST_POSTC	1083 / 476	22 / 0	0.024 / 0.017
ST_PREC	1462 / 503	37 / 0	0.027 / 0.016
ST_PREF	770 / 619	0 / 0	0.018 / 0.015
ST_PREM	117 / 114	0 / 0	0.018 / 0.017
STR	705 / 359	0 / 0	0.017 / 0.014
T_OCC	581 / 378	25 / 0	0.023 / 0.017
T_PAR	1010 / 426	0 / 0	0.020 / 0.016
T_POSTC	723 / 263	0 / 0	0.017 / 0.015
T_PREC	1110 / 463	6 / 0	0.022 / 0.014
T_PREF	739 / 579	0 / 0	0.019 / 0.015
T_PREM	39 / 146	0 / 0	0.014 / 0.014
UF	631 / 313	23 / 0	0.022 / 0.016

Table 2. Intersections of white matter tracts with significant fixels for correlations between FDC and reading skill. The number of fixels are present for two significance thresholds. For tracts that exist bilaterally, results are given in the form of L / R. Tracts in which the maximum effect size (ΔR^2_{adj}) exceeded 0.03 are designated with a bold font. This only happened in the left hemisphere. Tract masks are not mutually exclusive, and nearby tracts likely overlapped to various degrees. Abbreviations for the tracts in bold are as follows: AF - arcuate fasciculus; MLF - middle longitudinal fasciculus; SCP - superior cerebellar peduncles; SLF - superior longitudinal fasciculus. Please refer to Figure 3 of the *TractSeg* publication (***Wasserthal et al., 2018a***) for a full list of the tract abbreviations.

Discussion

In this study, we employed a method to study fiber-specific properties as they relate to single-word reading abilities and diagnoses of reading disabilities in children and adolescents. We hypothesized that fixel-based metrics would be sensitive to variation in reading abilities especially in the left arcuate fasciculus, left inferior fronto-occipital fasciculus, and cerebellum. Unlike recent cross-sectional studies of fractional anisotropy that yielded few-to-no regions exhibiting significant FA-reading relationships or group differences in FA (***Moreau et al., 2018***; ***Koirala et al., 2021***; ***Economou et al., 2022***; ***Meisler and Gabrieli, 2022***; ***Roy et al., 2022***), we found that higher FDC related to better single-word reading skills throughout the brain. However, FDC did not differ between those with and without reading disabilities. Although significant correlations were observed bilaterally, the strongest effect sizes were in the left hemisphere, and especially in temporoparietal and cerebellar white matter. The tracts most likely associated with the regions of strongest correlations were the left-hemisphere AF, SLF, MLF, and SCP.

It is encouraging that the fixel-based results highlighted left-hemisphere dorsal temporoparietal white matter, as its importance to reading and language has been well-established. The AF and SLF connect inferior frontal and temporoparietal gray matter regions that are essential for language and reading processing (***Catani et al., 2005***). Lesion symptom mapping studies have demonstrated that the AF and SLF are vital connections in the reading network (***Baldo et al., 2018***; ***Li et al., 2021***). These tracts, particularly in the left hemisphere, are associated with phonological processing skills (***Yeatman et al., 2011***), which are critical to reading (***Vellutino and Scanlon, 1987***) and impaired in dyslexia (***Swan and Goswami, 1997***). However, strongest effects were not found in reading-related tracts projecting from the occipital lobe, such as the inferior fronto-occipital fasciculus (IFOF) and inferior longitudinal fasciculus (ILF). Longitudinal studies have suggested these ventral tracts are more associated with visual orthographic, as opposed to phonological, processing (***Yeatman et al., 2012***; ***Vanderauwera et al., 2018***). Our results suggest that phonological skills, as opposed to lower-level visual and orthographic processing, may provide more of a bottleneck to single-word reading abilities in children. These results are supported by a large-scale longitudinal study finding that fractional anisotropy of the left AF, but not ILF, covaries with single-word reading skill over time (***Roy et al., 2022***). This notion is also consistent with a behavioral study demonstrating that orthographic skills are more related with reading longer passages, as opposed to single words (***Barker et al., 1992***). Thus, fixel-based analyses of skills relating to reading longer texts might instead highlight ventral tracts. We also note that the MLF intersected with the significant fixel clusters. This tract has received less attention due to a lack of clear characterization of its structure and function. However, some clinical cases suggest that the left MLF may be associated with imparied verbal-auditory learning and comprehension (***Latini et al., 2021***), which could be relevant to reading abilities. We reiterate that the tract masks largely overlapped and should not be used to make definitive associations between fixel-location and bundles, especially because tracts were defined in template, as opposed to native, space.

Our findings suggest that higher FDC in the superior cerebellar peduncles (SCP) is associated with better reading skills. Although the cerebellum is not commonly perceived

as a core hub in the reading network, theories of reading suggest the cerebellum has a role in fluent word recognition (***Alvarez and Fiez, 2018***; ***D'Mello et al., 2020***; ***Li et al., 2022***), and cerebellar deficits have been hypothesized as central impairments in dyslexia (***Nicolson et al., 2001***). In particular, the SCP contains efferent fibers that connect deep cerebellar nuclei to thalamic cortical regions. Previous studies suggest that fractional anisotropy of bilateral SCP inversely relates to reading skills (***Travis et al., 2015***; ***Bruckert et al., 2020***). We did not find an inverse relationship between FDC and reading abilities, although one should not *a priori* expect fractional anisotropy and FDC to covary. Our findings suggest that the cerebellum should remain a focus in studies of reading skills, especially since it is often cropped out of MRI acquisitions.

Our findings contribute to a growing list of cross-sectional studies suggesting that models more nuanced than the diffusion tensor better capture variance in reading skills (***Koirala et al., 2021***; ***Sihvonen et al., 2021***; ***Economou et al., 2022***). Unlike many prior studies we ran a whole-brain analysis instead of running statistics on metrics averaged within tracts. This has important implications for interpreting results. Our whole-brain findings suggest a relationship between reading skills and FDC in fixel-specific regions shared across participants. However, this does not preclude the possibility of tract-averaged diffusion metrics relating to reading skills, even among areas that yielded few significant fixels. A disruption in white matter leading to a deficit in reading might happen at any location along a tract, and variance in such locations across participants could lead to null findings on a fixel-by-fixel level. Whole-brain analyses are also prone to stricter correction for multiple tests. On the other hand, the spatial specificity achieved by whole-brain FBAs could be informative for speculating about the outcomes of white matter disruptions. White matter bundles do not only deliver signals from one end to the other; they branch off and synapse at multiple locations along its course. Thus, spatially specific disruptions of signal could have different downstream effects, warranting a more nuanced approach. The difference in our approach could explain why we found fewer negative associations between orientation dispersion index from NODDI, as well as no significant negative associations with neurite density index, compared to ***Koirala et al.*** (***2021***).

In our previous work (***Meisler and Gabrieli, 2022***), we correlated diffusion metrics with each TOWRE sub-test score individually. However, in the current study, we used the composite TOWRE measure as the phenotypic variable of interest. Our rationale in doing so is the same as in ***Sihvonen et al.*** (***2021***): A composite score is more stable, as it is more robust to variance due to temporary attention lapses which may only affect performance on one test. In addition, running fewer models mitigates the problem of multiple hypothesis testing. We acknowledge, however, that real word and pseudoword reading may rely on different skills. Pseudoword reading ability, for example, is considered a more pure gauge of phonological processing skills, because the novelty of these nonwords precludes one from relying on memorized representations. Given that the two sub-scores were highly correlated (Figure 2), we expect that models run on the individual sub-scores would have yielded similar results.

While our correlation tests did yield significant findings for FDC, the analogous comparison between typical and dyslexic groups did not. This could be in part due to fewer participants being included in the group analyses (total n = 672) compared to the con-

tinuous analyses (n = 983). It is also important to consider that collapsing participants into reading proficiency groups loses information about individual differences in reading ability. Group comparisons based on the same metric used in correlation analyses are inherently sacrificing statistical power from losing this individual variability. Although it is a worthwhile pursuit to investigate neurodevelopmental bases of dyslexia, which may be addressed by group comparisons, these questions may be better asked in pre-readers based on future reading outcomes (that is, comparing children who later do and do not develop typical reading skills). Studying pre-readers would rule-out concerns that findings are due to the consequences of developing typical or poor reading skills, as opposed to the etiology (***Protopapas and Parrila, 2018***, ***2019***), which is a concern for studies of late-stage readers. There has not yet been a fixel-based analysis in pre-readers, but other studies have found white matter microstructural alterations, largely in the left arcuate fasciculus, among pre-readers who have a genetic risk for dyslexia, lower pre-reading skills associated with risk for dyslexia, or future diagnoses of dyslexia (***Saygin et al., 2013***; ***Vandermosten et al., 2015***; ***Langer et al., 2017***; ***Vanderauwera et al., 2017***; ***Wang et al., 2017***; ***Yu et al., 2020***).

Our findings should be interpreted in the context of several limitations. First, it was not made available what specific criteria were used to diagnose reading disabilities. This is why we used stringent criteria based on clinical and cognitive assessments to define the RD group. Secondly, most participants in the Healthy Brain Network present with at least one psychological, learning, or neurodevelopmental disorder (***Alexander et al., 2017***). The diversity of the cohort, while perhaps more representative of a population, presents multiple phenotypic factors that could confound results. To maintain high statistical power and a diverse sample, we did not exclude participants based on the presence of other neurodevelopmental or learning disorders such as ADHD or specific language impairments. Next, since white matter bundles can have different shapes across participants (***Yeatman et al., 2011***; ***Wassermann et al., 2011***) and analyses are performed in a single template space, an effect in a region of fixels could be partially driven by global geometric variations across participants. Similarly, the fixel-to-tract attributions should be cautiously interpreted, since our tracts were delineated on the FOD template of 38 participants, and tract segmentations tend to overlap (***Schilling et al., 2022***). The b-value of 2000 s/mm^2, while higher than the b-value of typical DTI acquisitions, is not exceptionally large compared to the spectrum of values typically employed in FBA. Thus, our measures of FD, and therefore FDC as well, may have been partially undermined by contamination from extra-axonal signal (***Genc et al., 2020***). FDC, while interpreted as a measure of the ability of white matter to relay information (***Raffelt et al., 2017b***), has not yet been extensively validated against histological measures. Finally, our study is cross-sectional and correlational. Thus, it cannot be used to make causal conclusions of white matter's contributions to reading skills. We hope our work will inform future fixel-based investigations using longitudinal, mediation, modeling, or prediction approaches that can warrant stronger claims.

Conclusion

In the present study, we examined whether fixel-based metrics from 983 children and adolescents covaried with single-word reading abilities or were reduced among those with reading disabilities. We found that higher FDC related to better single-word reading abilities, but that FDC did not differ between children with and without reading disabilities. The strongest associations between FDC and reading aptitude were localized in left-hemisphere temporoparietal and cerebellar white matter, which is consistent with prior neuroanatomical studies of reading and literacy. The fixel-based analysis is a promising approach to investigating reading in future studies, capturing variance in reading skill when multiple other DWI-derived scalars fail to do so, and parameters of DWI acquisitions should be considered with this in mind.

Methods and Materials

Participants

We downloaded preprocessed DWI and phenotypic data from 2136 participants across the first eight data releases of the Healthy Brain Network (HBN) project (***Alexander et al., 2017***). Phenotypic data were accessed in accordance with a data use agreement provided by the Child Mind Institute. Preprocessed DWI data were provided as part of the HBN Preprocessed Open Diffusion Derivatives (HBN-POD2) data set (***Richie-Halford et al., 2022***). The Healthy Brain Network project was approved by the Chesapeake Institutional Review Board (now called Advarra, Inc.; https://www.advarra.com/). Informed consent was obtained from all participants ages 18 or older. For younger participants, written informed consent was collected from their legal guardians, and written assent was obtained from the participants. Detailed inclusion and exclusion criteria for the Healthy Brain Network data set are described in the project's publication (***Alexander et al., 2017***). Of note, each participant was fluent in English, had an IQ over 66, and did not have any physical or mental disorder precluding them from completing the full battery of scanning and behavioral examinations.

Several behavioral and cognitive evaluations were collected as part of HBN. Relevant to this study, participants completed the Test of Word Reading Efficiency 2nd edition (TOWRE; ***Torgesen et al.*** (***1999***)). The TOWRE consists of two subtests, Sight Word Efficiency (SWE) and Phonemic Decoding Efficiency (PDE). For these tests, each participant is shown a list of either real words (SWE) or pronounceable non-words / pseudowords (PDE) and asked to read the items aloud as quickly as possible. Raw scores are based on the number of items read correctly within the 45-second time limit and are then converted to an age-standardized score (population mean = 100, standard deviation = 15). A composite TOWRE score is calculated as the mean of the standardized PDE and SWE scores. Most participants also completed the Edinburgh Handedness Inventory (EHI; ***Oldfield*** (***1971***)), Barratt Simplified Measure of Social Status (BSMSS; ***Barratt*** (***2006***)) and Wechsler Intelligence Scale for Children 5th edition (WISC; ***Wechsler and Kodama*** (***1949***)).

After quality control (see *Data Inclusion and Quality Control* below), there were 983 participants ages 6-18 years old. We divided these participants into two groups based on diagnostic criteria and standardized reading scores (Figure 2). 102 participants were di-

agnosed with a "specific learning disability with impairment in reading" following the 5th edition of the Diagnostic and Statistical Manual for Mental Disorders (***Edition et al., 2013***) and scored ≤ 85 on both TOWRE subtests (age-standardized). These participants were placed in the reading disability (RD) group. 570 participants who were not diagnosed with a reading impairment and scored ≥ 90 on both TOWRE subtests (age-standardized) were placed in the typically reading (TR) group. The remaining 311 participants were not placed into either group, but were still included in the correlation analyses across all participants.

Neuroimaging Acquisition

Detailed scanner protocols for each site are published on the Healthy Brain Network project website (http://fcon_1000.projects.nitrc.org/indi/cmi_healthy_brain_network/File/mri/). Data were collected using either a 1.5T Siemens mobile scanner (Staten Island site) or a 3T Siemens MRI scanner (sites at Rutgers University Brain Imaging Center, Cornell Brain Imaging Center, and the City University of New York Advanced Science Research Center). All participants were scanned while wearing a standard Siemens 32-channel head coil. A high-resolution T1-weighted (T1w) image was collected for all participants, with parameters that slightly varied between sites. A diffusion kurtosis imaging scan was acquired with 1.8 mm isotropic voxel resolution, 1 b = 0 s/mm^2 image, and 64 noncollinear directions collected at b = 1000 s/mm^2 and b = 2000 s/mm^2. A pair of PEpolar fieldmaps were collected before the diffusion scan to quantify magnetic field susceptibility distortions.

Neuroimaging Minimal Preprocessing

Minimally preprocessed data was downloaded from HBN-POD2 and produced by *QSIPrep* (***Cieslak et al., 2021***) 0.12.1 (https://qsiprep.readthedocs.io/en/latest/), which is based on *Nipype* 1.5.1 (***Gorgolewski et al., 2011***, ***2018***) (RRID:SCR_002502). Many internal operations of *QSIPrep* use *Nilearn* 0.6.2 (***Abraham et al., 2014***) (RRID:SCR_001362) and *Dipy* (***Garyfallidis et al., 2014***). The following two sections contain text from boilerplates distributed by *QSIPrep* under a CC0 license with the expressed intention of being incorporated into manuscripts for transparency and reproducibility. We made minor changes for succinctness and completeness.

Anatomical Preprocessing

The T1w image was corrected for intensity non-uniformity (INU) using `N4BiasFieldCorrection` (***Tustison et al., 2010***) (ANTs 2.3.1), and used as T1w-reference throughout the workflow. The T1w-reference was then skull-stripped using `antsBrainExtraction.sh` (ANTs 2.3.1), using OASIS as target template. Brain tissue segmentation of cerebrospinal fluid (CSF), white-matter (WM) and gray-matter (GM) was performed on the brain-extracted T1w using `FAST` (***Zhang et al., 2001***) (FSL 6.0.3:b862cdd5, RRID:SCR_002823). Additionally, in order to calculate intracranial volumes, we ran `recon-all` (*FreeSurfer* 6.0.1, RRID:SCR_001847; ***Dale et al.*** (***1999***); ***Buckner et al.*** (***2004***); ***Fischl*** (***2012***)) as part of *sMRIPrep* 0.8.1 (***Esteban et al., 2021***) to reconstruct brain surfaces.

Diffusion Image Preprocessing

Denoising using `dwidenoise` (***Veraart et al., 2016***) was applied with settings based on developer recommendations. Gibbs unringing was performed using *MRtrix3*'s `mrdegibbs` (***Kellner et al., 2016***). Following unringing, B1 field inhomogeneity was corrected using `dwibiascorrect` from *MRtrix3* with the N4 algorithm (***Tustison et al., 2010***). After B1 bias correction, the mean intensity of the DWI series was adjusted so all the mean intensity of the b = 0 images matched across each separate DWI scanning sequence. *FSL* (version 6.0.3:b862cdd5)'s `eddy` was used for head motion correction and Eddy current correction (***Andersson and Sotiropoulos, 2016***). `eddy` was configured with a q-space smoothing factor of 10, a total of 5 iterations, and 1000 voxels used to estimate hyperparameters. A linear first level model and a linear second level model were used to characterize Eddy current-related spatial distortion. q-space coordinates were forcefully assigned to shells. Field offset was attempted to be separated from participant movement. Shells were aligned post-`eddy`. `eddy`'s outlier replacement was run (***Andersson et al., 2016***). Data were grouped by slice, only including values from slices determined to contain at least 250 intracerebral voxels. Groups deviating by more than 4 standard deviations from the prediction had their data replaced with imputed values. Here, b = 0 fieldmap images with reversed phase-encoding directions were used along with an equal number of b = 0 images extracted from the DWI scans. From these pairs the susceptibility-induced off-resonance field was estimated using a method similar to that described in ***Andersson et al.*** (***2003***). The fieldmaps were ultimately incorporated into the Eddy current and head motion correction interpolation. Final interpolation was performed using the `jac` method. The preprocessed DWI time-series were resampled to ACPC, and their corresponding gradient directions were rotated accordingly.

Fixel-Based Analyses (FBA)

Fixel Metric Calculations

Comprehensive details of this pipeline have been described elsewhere (***Raffelt et al., 2017b***). Preprocessed DWI volumes and brain masks were reoriented to the *FSL* standard orientation. The gradient table was correspondingly rotated with *MRtrix3*'s `dwigradcheck`. We then upsampled the DWI image and brain masks to 1.25 isotropic voxels. We extracted only the highest diffusion shell (b = 2000 s/mm^2, along with the b = 0 volumes) to proceed with estimating the constrained spherical deconvolution (CSD) fiber response functions and fiber orientation distributions (FODs), as to limit the influence of extra-axonal signal (***Genc et al., 2020***). Response functions for white matter, gray matter, and cerebrospinal fluid were estimated with *MRtrix3*'s unsupervised `dhollander` algorithm (***Dhollander et al., 2016***, ***2019***). For each tissue compartment, site-specific average fiber response functions were calculated (***Raffelt et al., 2012b***). Participant FODs for each tissue compartment were calculated using Single-Shell 3-Tissue CSD (SS3T-CSD) (***Dhollander and Connelly, 2016***) from *MRtrix3Tissue* (https://3Tissue.github.io), a fork of *MRtrix3* (***J-Donald et al., 2019***). FODs were normalized using log-domain intensity normalization (***Raffelt et al., 2017a***; ***Dhollander et al., 2021a***).

We then generated an unbiased study-specific FOD template, and warped individual participant FOD images to this template (***Raffelt et al., 2011***, ***2012a***). Due to the large

size of our participant cohort, we could not feasibly use all FOD images to generate a population template. To decide which participants were used to inform the template, we divided the age range of participants into 10 uniformly-spaced bins. In each age bin, we selected two males and two females. Within sex groupings, the participant in the TR and RD group with the highest quality control prediction score ("XGB score", see ***Richie-Halford et al.*** (***2022***)) was selected to be in the template. There were no females in the RD group among the two oldest age bins, so our template was composed of 38 participants. We implemented this method to make a robust template that was unbiased by sex and included representation from a wide range of ages and reading levels. All participant brain masks were warped to the template space. A whole-brain template-space analysis mask was calculated as the intersection of all of these warped masks, such that each region would contain data from all participants. Within this voxel-wise template mask, a whole-brain fixel-wise analysis mask was segmented from the FOD template.

Participant fixels were segmented from their warped FODs (***Smith et al., 2013***), and then reoriented and mapped to the template space. Fiber density (FD) was calculated for each fixel by taking the integral of its corresponding FOD lobes (***Raffelt et al., 2012b***). Fiber cross-sections (FC) were also calculated for each fixel, informed by the geometric distortions needed to warp from native-to-template space (***Raffelt et al., 2017b***). The product of the two metrics was also calculated (FDC) (***Raffelt et al., 2017b***). We applied a log transform to FC so it would be normally distributed and centered around 0. FDC was calculated before this log transformation was applied.

A whole-brain tractogram with 20 million streamlines was generated from the FOD template using seeds uniformly distributed across the template-space voxel-wise mask (***Tournier et al., 2010***). SIFT filtering (***Smith et al., 2013***) was applied to account for false positives in streamline generation (***Maier-Hein et al., 2017***), resulting in a pruned tractogram with 2 million streamlines. This was used to create a fixel-to-fixel connectivity matrix. This connectivity data was used to inform spatial smoothing of FD, log(FC), and FDC maps, such that smoothing at a given fixel only occurred within that fixel's fiber population, thus avoiding partial-volume effects or influences from crossing fibers (***Raffelt et al., 2015***).

Tract Segmentation

We extracted the three primary spherical harmonic peaks of the template FOD image within the voxel-wise brain mask (***Jeurissen et al., 2013***). These peaks were input to *TractSeg* 2.3 (***Wasserthal et al., 2018a***,b, ***2019***), a convolutional neural network-based tract segmentation and reconstruction pipeline that strikes a favorable balance between the subjectivity of manual delineation and objectivity of automated atlas-based tracking approaches (***Genc et al., 2020***). We created tractograms for all 72 fiber-bundles produced by *TractSeg*. We generated 10000 streamlines per tract (up from the default of 2000) to reduce inter-run variability from the stochastic nature of reconstruction. From each set of fiber bundle streamlines, we created a corresponding fixel tract density map, which we binarized to create tract fixel masks.

Statistics

We considered a diverse set of potential confounds to include in our statistical models. These included age (***Genc et al., 2018***; ***Dimond et al., 2020***), sex (***Lyon et al., 2019***; ***Kirkovski et al., 2020***), handedness, socioeconomic status (SES) as indexed by the average years of parental education from the BSMSS, visuospatial IQ index from the WISC (***Ramus et al., 2018***), globally-averaged fixel metrics (gFD, gFC), log-transformed intracranial volume (ICV) (***Smith et al., 2019***), and scanning site (***Schilling et al., 2021b***). We also considered multiple quality covariates, including mean framewise displacement, and neighbor correlation (***Yeh et al.*** (***2019***)). The machine-learning based quality score distribution from ***Richie-Halford et al.*** (***2022***) was skewed towards 1 and not normally distributed, and thus was not a good candidate confound. Since gFD and gFC are calculated within fixels, and fixels are only segmented in white matter, differences in white matter volumetric proportions should not influence global fixel-metrics. As exploratory analyses, we ran Spearman correlations between all continuous variables to inform our decision of model covariates and look for well-established trends in behavioral and neuroimaging metrics, validating the data collection procedures (Fig. S1).

To run our statistical models, we used *ModelArray* 0.1.0 (***Zhao et al., 2022***). This R-based software package minimizes memory consumption to allow analysis of all participants and enables generalized additive modeling (GAM) on fixel data, which is especially useful for cohorts with a wide age-range (***Bethlehem et al., 2022***). We ran two models for our primary analyses: a regression of FDC against the age-standardized TOWRE composite score, and a comparison of FDC between the TR and RD groups. We restrict our primary analyses to FDC based on recent guidance surrounding the control of false positives in FBA (***Smith et al., 2021***), but we also ran analogous models for FD and log(FC) to explore the contributions of fiber microstructure and morphometry in a *post-hoc* fashion. Model confounds included a smooth spline fit for age and linear fits for sex, site, quality (neighbor correlation), and log(ICV). Log(ICV) was not included as a covariate for models related to FD (***Smith et al., 2019***). Categorical variables (group, sex, and site) were coded as factors, and continuous variables (TOWRE scores, neighbor correlation, age, and ICV) were mean-centered and rescaled to unit variance to mitigate concerns of multicollinearity and poor design matrix conditioning. Effect sizes for the predictors of interest (TOWRE score or group label) were calculated as the difference in adjusted R^2 coefficients (ΔR^2_{adj}) between the full statistical model fit and the fit of a reduced model without the primary predictor variable. P-values were corrected across the brain using Benjamini-Hochberg FDR correction (***Benjamini and Hochberg, 1995***). To ascribe significant fixels to tracts, we intersected significant fixels ($q_{FDR} < 0.05$) and the binarized tract masks. We note that tract masks tended to overlap (***Schilling et al., 2022***), so a single fixel could be associated with multiple fiber bundles.

We also ran similar models relating reading abilities with various scalar maps from diffusion tensor models, diffusion kurtosis models, and NODDI models. Details of these analyses are in the supplementary materials (Figure S7).

Data Inclusion and Quality Control

We downloaded preprocessed DWI (***Richie-Halford et al., 2022***) and phenotypic data from 2136 participants across the first eight data releases of the Healthy Brain Network (HBN) project (***Alexander et al., 2017***). HBN-POD2 distributes a quality metric accompanying each image that predicts the probability that the image would pass manual expert quality review ("`xgb_qc_score`", or "`dl_qc_score`" if the former score was not available) (***Richie-Halford et al., 2022***). It ranges from 0 (no chance of passing expert review) to 1 (image will definitely pass expert review). We excluded any participants with a quality score of less than 0.5. Twenty different DWI acquisition parameters were present across participants (***Covitz et al., 2022***; ***Richie-Halford et al., 2022***). We only included participants who had images acquired with the most common acquisition parameters in their site ("`SITE_64dir_most_common`"). We also excluded any participant who: 1) was outside ages 6-18; 2) had missing basic demographic or TOWRE scores; or 3) failed *FreeSurfer* reconstruction. Based on these criteria, 986 participants advanced to the fixel-based analysis. Fiber response functions could not be obtained for two of these participants due to non-positive tissue balance factors. After registering the participant FODs to the template FOD, we overlaid each participant's registered brain mask on top of the registered FOD image. This revealed 1 participant with an unsuccessful registration to template space who was excluded from analyses. Therefore, a total of n = 983 participants (570 TR, 102 RD, 311 other) passed all quality control procedures and were included in subsequent analyses.

Data and Code Availability

Preprocessed neuroimaging data can be downloaded following directions from the HBN-POD2 manuscript (***Richie-Halford et al., 2022***), and phenotypic data can be collected following directions on the Healthy Brain Network data portal (http://fcon_1000.projects.nitrc.org/indi/cmi_healthy_brain_network/index.html) after signing a data use agreement. All instructions and code for further processing data and running the statistical models can be found at https://github.com/smeisler/Meisler_Reading_FBA. With minimal modification, the neuroimaging processing code should be able to run on most BIDS-compliant data sets using the SLURM job scheduler (***Yoo et al., 2003***). Some softwares we used were distributed as Docker (***Merkel, 2014***) containers, then compiled and run with Singularity 3.9.5 (***Kurtzer et al., 2017***):

- *QSIPrep* 0.15.3 (`singularity build qsiprep.simg docker://pennbbl/qsiprep:0.15.3`)
- *TractSeg* 2.3 (`singularity build tractseg.simg docker://wasserth/tractseg:master`)
- *MRtrix3* 3.0.3 (`singularity build mrtrix.simg docker://mrtrix3/mrtrix3:3.0.3`)
- *MRtrix3Tissue* 5.2.9 (`singularity build mrtrix3t.simg docker://kaitj/mrtrix3tissue:v5.2.9`)
- *sMRIPrep* 0.8.1 (`singularity build smriprep.simg docker://nipreps/smriprep:0.8.1`)
- *FSL* 6.0.4 (`singularity build fsl.simg`

`docker://brainlife/fsl:6.0.4-patched`)

We encourage anyone to use the latest stable releases of these softwares.

CRediT Authorship Contributions

Steven L. Meisler: Conceptualization, Formal analysis, Investigation, Methodology, Visualization, Writing - original draft, Writing - review & editing. **John D.E. Gabrieli:** Conceptualization, Supervision, Writing - original draft, Writing - review & editing.

Acknowledgements

We thank the Child Mind Institute for their diligence in collecting the neuroimaging data and the authors of the HBN-POD2 manuscript for sharing the preprocessed derivatives. We thank all of the participants and their families for volunteering their time to be involved in the Healthy Brain Network. We thank Chenying Zhao, Matt Cieslak, and Theodore Satterthwaite for developing and guiding the use of the *ModelArray* software which made this study possible.

This work was funded by The National Institute on Deafness and Other Communication Disorders (NIDCD) (grant numbers 5T32DC000038-29 and 5T32DC000038-30), the Halis Family Foundation, and Reach Every Reader, a grant supported by the Chan Zuckerberg Foundation.

Competing Interests

The authors have no competing interests to declare.

References

Abraham A, Pedregosa F, Eickenberg M, Gervais P, Mueller A, Kossaifi J, Gramfort A, Thirion B, Varoquaux G. Machine learning for neuroimaging with scikit-learn. Frontiers in Neuroinformatics. 2014; 8. https://www.frontiersin.org/articles/10.3389/fninf.2014.00014/full, doi: 10.3389/fninf.2014.00014.

Alexander LM, Escalera J, Ai L, Andreotti C, Febre K, Mangone A, Vega-Potler N, Langer N, Alexander A, Kovacs M, et al. An open resource for transdiagnostic research in pediatric mental health and learning disorders. Scientific data. 2017; 4(1):1–26.

Alonso-Ortiz E, Levesque IR, Pike GB. MRI-based myelin water imaging: a technical review. Magnetic resonance in medicine. 2015; 73(1):70–81.

Alvarez TA, Fiez JA. Current perspectives on the cerebellum and reading development. Neuroscience & Biobehavioral Reviews. 2018; 92:55–66.

Andersson JL, Graham MS, Zsoldos E, Sotiropoulos SN. Incorporating outlier detection and replacement into a non-parametric framework for movement and distortion correction of diffusion MR images. Neuroimage. 2016; 141:556–572.

Andersson JL, Skare S, Ashburner J. How to correct susceptibility distortions in spin-echo echo-planar images: application to diffusion tensor imaging. Neuroimage. 2003; 20(2):870–888.

622 **Andersson JL**, Sotiropoulos SN. An integrated approach to correction for off-resonance effects
623 and subject movement in diffusion MR imaging. Neuroimage. 2016; 125:1063–1078.

624 **Baldo JV**, Kacinik N, Ludy C, Paulraj S, Moncrief A, Piai V, Curran B, Herron T, Dronkers NF, et al.
625 Voxel-based lesion analysis of brain regions underlying reading and writing. Neuropsychologia.
626 2018; 115:51–59.

627 **Barker TA**, Torgesen JK, Wagner RK. The role of orthographic processing skills on five different
628 reading tasks. Reading Research Quarterly. 1992; p. 335–345.

629 **Barratt W**. The Barratt simplified measure of social status (BSMSS). Indiana State University. 2006;
630 .

631 **Basser PJ**, Mattiello J, LeBihan D. MR diffusion tensor spectroscopy and imaging. Biophysical
632 journal. 1994; 66(1):259–267.

633 **Basser PJ**, Pierpaoli C. Microstructural and physiological features of tissues elucidated by
634 quantitative-diffusion-tensor MRI. Journal of magnetic resonance. 1996; 213(2):560–570.

635 **Beaulieu C**. Diffusion MRI: from quantitative measurement to in vivo neuroanatomy. Academic
636 Press; 2009.

637 **Beaulieu C**, Yip E, Low PB, Mädler B, Lebel CA, Siegel L, Mackay AL, Laule C. Myelin Water Imaging
638 Demonstrates Lower Brain Myelination in Children and Adolescents With Poor Reading Ability.
639 Frontiers in Human Neuroscience. 2020; p. 405.

640 **Begg CB**. Publication bias. The handbook of research synthesis. 1994; 25:299–409.

641 **Behrens TE**, Berg HJ, Jbabdi S, Rushworth MF, Woolrich MW. Probabilistic diffusion tractography
642 with multiple fibre orientations: What can we gain? Neuroimage. 2007; 34(1):144–155.

643 **Ben-Shachar M**, Dougherty RF, Wandell BA. White matter pathways in reading. Current opinion
644 in neurobiology. 2007; 17(2):258–270.

645 **Benjamini Y**, Hochberg Y. Controlling the false discovery rate: a practical and powerful approach
646 to multiple testing. Journal of the Royal statistical society: series B (Methodological). 1995;
647 57(1):289–300.

648 **Bethlehem RA**, Seidlitz J, White SR, Vogel JW, Anderson KM, Adamson C, Adler S, Alexopoulos GS,
649 Anagnostou E, Areces-Gonzalez A, et al. Brain charts for the human lifespan. Nature. 2022; p.
650 1–11.

651 **Birkl C**, Doucette J, Fan M, Hernández-Torres E, Rauscher A. Myelin water imaging depends on
652 white matter fiber orientation in the human brain. Magnetic resonance in medicine. 2021;
653 85(4):2221–2231.

654 **Bruckert L**, Travis KE, Mezer AA, Ben-Shachar M, Feldman HM. Associations of reading efficiency
655 with white matter properties of the cerebellar peduncles in children. The Cerebellum. 2020;
656 19(6):771–777.

657 **Buckner RL**, Head D, Parker J, Fotenos AF, Marcus D, Morris JC, Snyder AZ. A unified approach for
658 morphometric and functional data analysis in young, old, and demented adults using automated
659 atlas-based head size normalization: reliability and validation against manual measurement of
660 total intracranial volume. Neuroimage. 2004; 23(2):724–738.

661 **Carter JC**, Lanham DC, Cutting LE, Clements-Stephens AM, Chen X, Hadzipasic M, Kim J, Denckla
662 MB, Kaufmann WE. A dual DTI approach to analyzing white matter in children with dyslexia.
663 Psychiatry Research: Neuroimaging. 2009; 172(3):215–219.

664 **Catani M**, Jones DK, Ffytche DH. Perisylvian language networks of the human brain. Annals of
665 Neurology: Official Journal of the American Neurological Association and the Child Neurology
666 Society. 2005; 57(1):8–16.

667 **Cattinelli I**, Borghese NA, Gallucci M, Paulesu E. Reading the reading brain: a new meta-analysis
668 of functional imaging data on reading. Journal of neurolinguistics. 2013; 26(1):214–238.

669 **Christodoulou JA**, Murtagh J, Cyr A, Perrachione TK, Chang P, Halverson K, Hook P, Yendiki A, Ghosh
670 S, Gabrieli JD. Relation of white-matter microstructure to reading ability and disability in begin-
671 ning readers. Neuropsychology. 2017; 31(5):508.

672 **Cieslak M**, Cook PA, He X, Yeh FC, Dhollander T, Adebimpe A, Aguirre GK, Bassett DS, Betzel RF,
673 Bourque J, et al. QSIPrep: an integrative platform for preprocessing and reconstructing diffusion
674 MRI data. Nature methods. 2021; 18(7):775–778.

675 **Covitz S**, Tapera T, Adebimpe A, Alexander-Bloch A, Bertolero MA, Feczko E, Franco AR, Gur RE,
676 Gur RC, Hendrickson T, et al. Curation of BIDS (CuBIDS): a workflow and software package for
677 streamlining reproducible curation of large BIDS datasets. bioRxiv. 2022; .

678 **Daducci A**, Canales-Rodríguez EJ, Zhang H, Dyrby TB, Alexander DC, Thiran JP. Accelerated mi-
679 crostructure imaging via convex optimization (AMICO) from diffusion MRI data. Neuroimage.
680 2015; 105:32–44.

681 **Dale AM**, Fischl B, Sereno MI. Cortical surface-based analysis: I. Segmentation and surface recon-
682 struction. Neuroimage. 1999; 9(2):179–194.

683 **Dhollander T**, Tabbara R, Rosnarho-Tornstrand J, Tournier J, Raffelt D, Connelly A. Multi-tissue
684 log-domain intensity and inhomogeneity normalisation for quantitative apparent fibre density.
685 Proceedings of the 29th International Society of Magnetic Resonance in Medicine. 2021; .

686 **Dhollander T**, Clemente A, Singh M, Boonstra F, Civier O, Duque JD, Egorova N, Enticott P, Fuelscher
687 I, Gajamange S, et al. Fixel-based analysis of diffusion MRI: methods, applications, challenges and
688 opportunities. NeuroImage. 2021; p. 118417.

689 **Dhollander T**, Connelly A. A novel iterative approach to reap the benefits of multi-tissue CSD from
690 just single-shell (+ b= 0) diffusion MRI data. In: *Proc ISMRM*, vol. 24; 2016. p. 3010.

691 **Dhollander T**, Mito R, Raffelt D, Connelly A. Improved white matter response function estimation
692 for 3-tissue constrained spherical deconvolution. In: *Proc. Intl. Soc. Mag. Reson. Med*; 2019. p. 555.

693 **Dhollander T**, Raffelt D, Connelly A. Unsupervised 3-tissue response function estimation from
694 single-shell or multi-shell diffusion MR data without a co-registered T1 image. In: *ISMRM Work-*
695 *shop on Breaking the Barriers of Diffusion MRI*, vol. 5; 2016. p. 5.

696 **Dimond D**, Rohr CS, Smith RE, Dhollander T, Cho I, Lebel C, Dewey D, Connelly A, Bray S. Early
697 childhood development of white matter fiber density and morphology. NeuroImage. 2020;
698 210:116552.

699 **D'Mello AM**, Centanni TM, Gabrieli JD, Christodoulou JA. Cerebellar contributions to rapid semantic
700 processing in reading. Brain and language. 2020; 208:104828.

Economou M, Billiet T, Wouters J, Ghesquière P, Vanderauwera J, Vandermosten M. Myelin water fraction in relation to fractional anisotropy and reading in 10-year-old children. Brain Structure and Function. 2022; p. 1–9.

Edition F, et al. Diagnostic and statistical manual of mental disorders. Am Psychiatric Assoc. 2013; 21.

Epelbaum S, Pinel P, Gaillard R, Delmaire C, Perrin M, Dupont S, Dehaene S, Cohen L. Pure alexia as a disconnection syndrome: new diffusion imaging evidence for an old concept. cortex. 2008; 44(8):962–974.

Esteban O, Markiewicz C, Blair R, Poldrack R, Gorgolewski K, sMRIPrep: Structural MRI PREProcessing workflows; 2021.

Farquharson S, Tournier JD, Calamante F, Fabinyi G, Schneider-Kolsky M, Jackson GD, Connelly A. White matter fiber tractography: why we need to move beyond DTI. Journal of neurosurgery. 2013; 118(6):1367–1377.

Fields RD. A new mechanism of nervous system plasticity: activity-dependent myelination. Nature Reviews Neuroscience. 2015; 16(12):756–767.

Fischl B. FreeSurfer. Neuroimage. 2012; 62(2):774–781.

Friedrich P, Fraenz C, Schlüter C, Ocklenburg S, Mädler B, Güntürkün O, Genç E. The relationship between axon density, myelination, and fractional anisotropy in the human Corpus callosum. Cerebral Cortex. 2020; 30(4):2042–2056.

Frye RE, Hasan K, Xue L, Strickland D, Malmberg B, Liederman J, Papanicolaou A. Splenium microstructure is related to two dimensions of reading skill. Neuroreport. 2008; 19(16):1627.

Frye RE, Liederman J, Hasan KM, Lincoln A, Malmberg B, McLean III J, Papanicolaou A. Diffusion tensor quantification of the relations between microstructural and macrostructural indices of white matter and reading. Human brain mapping. 2011; 32(8):1220–1235.

Garyfallidis E, Brett M, Amirbekian B, Rokem A, Van Der Walt S, Descoteaux M, Nimmo-Smith I. Dipy, a library for the analysis of diffusion MRI data. Frontiers in neuroinformatics. 2014; 8:8.

Geeraert BL, Chamberland M, Lebel RM, Lebel C. Multimodal principal component analysis to identify major features of white matter structure and links to reading. PloS one. 2020; 15(8):e0233244.

Genc S, Smith RE, Malpas CB, Anderson V, Nicholson JM, Efron D, Sciberras E, Seal ML, Silk TJ. Development of white matter fibre density and morphology over childhood: A longitudinal fixel-based analysis. Neuroimage. 2018; 183:666–676.

Genc S, Tax CM, Raven EP, Chamberland M, Parker GD, Jones DK. Impact of b-value on estimates of apparent fibre density. Human brain mapping. 2020; 41(10):2583–2595.

Gorgolewski K, Burns CD, Madison C, Clark D, Halchenko YO, Waskom ML, Ghosh S. Nipype: a flexible, lightweight and extensible neuroimaging data processing framework in Python. Frontiers in Neuroinformatics. 2011; 5:13. doi: 10.3389/fninf.2011.00013.

Gorgolewski KJ, Esteban O, Markiewicz CJ, Ziegler E, Ellis DG, Notter MP, Jarecka D, Johnson H, Burns C, Manhães-Savio A, Hamalainen C, Yvernault B, Salo T, Jordan K, Goncalves M, Waskom M, Clark D, Wong J, Loney F, Modat M, et al. Nipype. Software. 2018; doi: 10.5281/zenodo.596855.

Hagmann P, Jonasson L, Maeder P, Thiran JP, Wedeen VJ, Meuli R. Understanding diffusion MR imaging techniques: from scalar diffusion-weighted imaging to diffusion tensor imaging and beyond. Radiographics. 2006; 26(suppl_1):S205–S223.

Hastie TJ, Tibshirani RJ. Generalized additive models. Routledge; 1990.

Henriques RN, Correia MM, Marrale M, Huber E, Kruper J, Koudoro S, Yeatman JD, Garyfallidis E, Rokem A. Diffusional kurtosis imaging in the diffusion imaging in python project. Frontiers in Human Neuroscience. 2021; p. 390.

Horowitz-Kraus T, Grainger M, DiFrancesco M, Vannest J, Holland SK. Right is not always wrong: DTI and fMRI evidence for the reliance of reading comprehension on language-comprehension networks in the right hemisphere. Brain imaging and behavior. 2015; 9(1):19–31.

J-Donald, Smith R, Raffelt D, Tabbara R, Dhollander T, Pietsch M, Christiaens D, Jeurissen B, Yeh CH, Connelly A. MRtrix3: A fast, flexible and open software framework for medical image processing and visualisation. NeuroImage. 2019; 202:116137.

Jeurissen B, Leemans A, Tournier JD, Jones DK, Sijbers J. Investigating the prevalence of complex fiber configurations in white matter tissue with diffusion magnetic resonance imaging. Human brain mapping. 2013; 34(11):2747–2766.

Johansen-Berg H, Behrens TE. Diffusion MRI: from quantitative measurement to in vivo neuroanatomy. Academic Press; 2013.

Jones DK, Knösche TR, Turner R. White matter integrity, fiber count, and other fallacies: the do's and don'ts of diffusion MRI. Neuroimage. 2013; 73:239–254.

Kellner E, Dhital B, Kiselev VG, Reisert M. Gibbs-ringing artifact removal based on local subvoxel-shifts. Magnetic resonance in medicine. 2016; 76(5):1574–1581.

Kirkovski M, Fuelscher I, Hyde C, Donaldson PH, Ford TC, Rossell SL, Fitzgerald PB, Enticott PG. Fixel Based Analysis Reveals Atypical White Matter Micro-and Macrostructure in Adults With Autism Spectrum Disorder: An Investigation of the Role of Biological Sex. Frontiers in integrative neuroscience. 2020; 14:40.

Klingberg T, Hedehus M, Temple E, Salz T, Gabrieli JD, Moseley ME, Poldrack RA. Microstructure of temporo-parietal white matter as a basis for reading ability: evidence from diffusion tensor magnetic resonance imaging. Neuron. 2000; 25(2):493–500.

Koirala N, Perdue MV, Su X, Grigorenko EL, Landi N. Neurite density and arborization is associated with reading skill and phonological processing in children. NeuroImage. 2021; 241:118426.

Kurtzer GM, Sochat V, Bauer MW. Singularity: Scientific containers for mobility of compute. PloS one. 2017; 12(5):e0177459.

Landi N, Frost SJ, Mencl WE, Sandak R, Pugh KR. Neurobiological bases of reading comprehension: Insights from neuroimaging studies of word-level and text-level processing in skilled and impaired readers. Reading & Writing Quarterly. 2013; 29(2):145–167.

Langer N, Peysakhovich B, Zuk J, Drottar M, Sliva DD, Smith S, Becker BL, Grant PE, Gaab N. White matter alterations in infants at risk for developmental dyslexia. Cerebral Cortex. 2017; 27(2):1027–1036.

Latini F, Trevisi G, Fahlström M, Jemstedt M, Alberius Munkhammar Å, Zetterling M, Hesselager G, Ryttlefors M. New insights into the anatomy, connectivity and clinical implications of the middle longitudinal fasciculus. Frontiers in neuroanatomy. 2021; 14:610324.

Lazari A, Lipp I. Can MRI measure myelin? Systematic review, qualitative assessment, and meta-analysis of studies validating microstructural imaging with myelin histology. Neuroimage. 2021; 230:117744.

Lazari A, Salvan P, Cottaar M, Papp D, van der Werf OJ, Johnstone A, Sanders ZB, Sampaio-Baptista C, Eichert N, Miyamoto K, et al. Reassessing associations between white matter and behaviour with multimodal microstructural imaging. Cortex. 2021; .

Lebel C, Shaywitz B, Holahan J, Shaywitz S, Marchione K, Beaulieu C. Diffusion tensor imaging correlates of reading ability in dysfluent and non-impaired readers. Brain and language. 2013; 125(2):215–222.

Li H, Yuan Q, Luo YJ, Tao W. A new perspective for understanding the contributions of the cerebellum to reading: The cerebro-cerebellar mapping hypothesis. Neuropsychologia. 2022; p. 108231.

Li M, Song L, Zhang Y, Han Z. White matter network of oral word reading identified by network-based lesion-symptom mapping. Iscience. 2021; 24(8):102862.

Lyon M, Welton T, Varda A, Maller JJ, Broadhouse K, Korgaonkar MS, Koslow SH, Williams LM, Gordon E, Rush AJ, et al. Gender-specific structural abnormalities in major depressive disorder revealed by fixel-based analysis. NeuroImage: Clinical. 2019; 21:101668.

Maier-Hein KH, Neher PF, Houde JC, Côté MA, Garyfallidis E, Zhong J, Chamberland M, Yeh FC, Lin YC, Ji Q, et al. The challenge of mapping the human connectome based on diffusion tractography. Nature communications. 2017; 8(1):1–13.

Meisler SL, Gabrieli JD. A Large-Scale Investigation of White Matter Microstructural Associations with Reading Ability. NeuroImage. 2022; p. 118909.

Merkel D. Docker: lightweight linux containers for consistent development and deployment. Linux journal. 2014; 2014(239):2.

Moreau D, Stonyer JE, McKay NS, Waldie KE. No evidence for systematic white matter correlates of dyslexia: an activation likelihood estimation meta-analysis. Brain research. 2018; 1683:36–47.

Murphy KA, Jogia JR, Talcott JB. On the neural basis of word reading: A meta-analysis of fMRI evidence using activation likelihood estimation. Journal of Neurolinguistics. 2019; 49:71–83.

Nicolson RI, Fawcett AJ, Dean P. Developmental dyslexia: the cerebellar deficit hypothesis. Trends in neurosciences. 2001; 24(9):508–511.

Oldfield RC. The assessment and analysis of handedness: the Edinburgh inventory. Neuropsychologia. 1971; 9(1):97–113.

Protopapas A, Parrila R. Is dyslexia a brain disorder? Brain sciences. 2018; 8(4):61.

Protopapas A, Parrila R. Dyslexia: Still not a neurodevelopmental disorder. Brain sciences. 2019; 9(1):9.

Raffelt D, Dhollander T, Tournier JD, Tabbara R, Smith RE, Pierre E, Connelly A. Bias field correction and intensity normalisation for quantitative analysis of apparent fibre density. In: *Proc. Intl. Soc. Mag. Reson. Med*, vol. 25; 2017. p. 3541.

Raffelt D, Tournier JD, Crozier S, Connelly A, Salvado O. Reorientation of fiber orientation distributions using apodized point spread functions. Magnetic Resonance in Medicine. 2012; 67(3):844–855.

Raffelt D, Tournier JD, Fripp J, Crozier S, Connelly A, Salvado O. Symmetric diffeomorphic registration of fibre orientation distributions. NeuroImage. 2011; 56(3):1171–1180.

Raffelt D, Tournier JD, Rose S, Ridgway GR, Henderson R, Crozier S, Salvado O, Connelly A. Apparent fibre density: a novel measure for the analysis of diffusion-weighted magnetic resonance images. Neuroimage. 2012; 59(4):3976–3994.

Raffelt DA, Smith RE, Ridgway GR, Tournier JD, Vaughan DN, Rose S, Henderson R, Connelly A. Connectivity-based fixel enhancement: Whole-brain statistical analysis of diffusion MRI measures in the presence of crossing fibres. Neuroimage. 2015; 117:40–55.

Raffelt DA, Tournier JD, Smith RE, Vaughan DN, Jackson G, Ridgway GR, Connelly A. Investigating white matter fibre density and morphology using fixel-based analysis. Neuroimage. 2017; 144:58–73.

Ramus F, Altarelli I, Jednoróg K, Zhao J, Di Covella LS. Neuroanatomy of developmental dyslexia: Pitfalls and promise. Neuroscience & Biobehavioral Reviews. 2018; 84:434–452.

Rauschecker AM, Deutsch GK, Ben-Shachar M, Schwartzman A, Perry LM, Dougherty RF. Reading impairment in a patient with missing arcuate fasciculus. Neuropsychologia. 2009; 47(1):180–194.

Richie-Halford A, Cieslak M, Ai L, Caffarra S, Covitz S, Franco AR, Karipidis II, Kruper J, Milham M, Avelar-Pereira B, et al. An open, analysis-ready, and quality controlled resource for pediatric brain white-matter research. bioRxiv. 2022; .

Richlan F, Kronbichler M, Wimmer H. Structural abnormalities in the dyslexic brain: A meta-analysis of voxel-based morphometry studies. Human brain mapping. 2013; 34(11):3055–3065.

Riffert TW, Schreiber J, Anwander A, Knösche TR. Beyond fractional anisotropy: extraction of bundle-specific structural metrics from crossing fiber models. Neuroimage. 2014; 100:176–191.

Roy E, Richie-Halford A, Kruper J, Narayan M, Bloom D, Brown TT, Jernigan TL, McCandliss BD, Rokem A, Yeatman JD. White matter and literacy: a dynamic system in flux. bioRxiv. 2022; .

Saygin ZM, Norton ES, Osher DE, Beach SD, Cyr AB, Ozernov-Palchik O, Yendiki A, Fischl B, Gaab N, Gabrieli JD. Tracking the roots of reading ability: white matter volume and integrity correlate with phonological awareness in prereading and early-reading kindergarten children. Journal of Neuroscience. 2013; 33(33):13251–13258.

Schilling KG, Rheault F, Petit L, Hansen CB, Nath V, Yeh FC, Girard G, Barakovic M, Rafael-Patino J, Yu T, et al. Tractography dissection variability: what happens when 42 groups dissect 14 white matter bundles on the same dataset? NeuroImage. 2021; p. 118502.

Schilling KG, Tax CM, Rheault F, Hansen C, Yang Q, Yeh FC, Cai L, Anderson AW, Landman BA. Fiber tractography bundle segmentation depends on scanner effects, vendor effects, acquisition resolution, diffusion sampling scheme, diffusion sensitization, and bundle segmentation workflow. NeuroImage. 2021; 242:118451.

Schilling KG, Tax CM, Rheault F, Landman BA, Anderson AW, Descoteaux M, Petit L. Prevalence of white matter pathways coming into a single white matter voxel orientation: The bottleneck issue in tractography. Human brain mapping. 2022; 43(4):1196–1213.

Shemesh N. Axon diameters and myelin content modulate microscopic fractional anisotropy at short diffusion times in fixed rat spinal cord. Frontiers in Physics. 2018; 6:49.

Sihvonen AJ, Virtala P, Thiede A, Laasonen M, Kujala T. Structural white matter connectometry of reading and dyslexia. NeuroImage. 2021; 241:118411.

Smith R, Dhollander T, Connelly A. On the regression of intracranial volume in fixel-based analysis. Proc Int Soc Magn Reson Med Sci Meet Exhib. 2019; .

Smith R, Christiaens D, Jeurissen B, Pietsch M, Vaughan D, Jackson G, et al. On false positive control in Fixel-Based Analysis. Proceeding of the 27th International Society of Magnetic Resonance in Medicine ISMRM. 2021; .

Smith RE, Tournier JD, Calamante F, Connelly A. SIFT: Spherical-deconvolution informed filtering of tractograms. Neuroimage. 2013; 67:298–312.

Swan D, Goswami U. Phonological awareness deficits in developmental dyslexia and the phonological representations hypothesis. Journal of experimental child psychology. 1997; 66(1):18–41.

Torgesen JK, Rashotte CA, Wagner RK. TOWRE: Test of word reading efficiency. Psychological Corporation Toronto, Ontario; 1999.

Tournier JD, Calamante F, Connelly A. Robust determination of the fibre orientation distribution in diffusion MRI: non-negativity constrained super-resolved spherical deconvolution. Neuroimage. 2007; 35(4):1459–1472.

Tournier JD, Calamante F, Connelly A, et al. Improved probabilistic streamlines tractography by 2nd order integration over fibre orientation distributions. In: *Proceedings of the international society for magnetic resonance in medicine*, vol. 1670 John Wiley & Sons, Inc. New Jersey, USA; 2010. .

Travis KE, Leitner Y, Feldman HM, Ben-Shachar M. Cerebellar white matter pathways are associated with reading skills in children and adolescents. Human brain mapping. 2015; 36(4):1536–1553.

Tustison NJ, Avants BB, Cook PA, Zheng Y, Egan A, Yushkevich PA, Gee JC. N4ITK: Improved N3 Bias Correction. IEEE Transactions on Medical Imaging. 2010; 29(6):1310–1320. doi: 10.1109/TMI.2010.2046908.

Vanderauwera J, De Vos A, Forkel SJ, Catani M, Wouters J, Vandermosten M, Ghesquière P. Neural organization of ventral white matter tracts parallels the initial steps of reading development: a DTI tractography study. Brain and Language. 2018; 183:32–40.

Vanderauwera J, Wouters J, Vandermosten M, Ghesquière P. Early dynamics of white matter deficits in children developing dyslexia. Developmental cognitive neuroscience. 2017; 27:69–77.

Vandermosten M, Boets B, Wouters J, Ghesquière P. A qualitative and quantitative review of diffusion tensor imaging studies in reading and dyslexia. Neuroscience & Biobehavioral Reviews. 2012; 36(6):1532–1552.

Vandermosten M, Vanderauwera J, Theys C, De Vos A, Vanvooren S, Sunaert S, Wouters J, Ghesquière P. A DTI tractography study in pre-readers at risk for dyslexia. Developmental cognitive neuroscience. 2015; 14:8–15.

Vellutino FR, Scanlon DM. Phonological coding, phonological awareness, and reading ability: Evidence from a longitudinal and experimental study. Merrill-Palmer Quarterly (1982-). 1987; p. 321–363.

Veraart J, Novikov DS, Christiaens D, Ades-Aron B, Sijbers J, Fieremans E. Denoising of diffusion MRI using random matrix theory. NeuroImage. 2016; 142:394–406.

Vos SB, Jones DK, Viergever MA, Leemans A. Partial volume effect as a hidden covariate in DTI analyses. Neuroimage. 2011; 55(4):1566–1576.

Wandell BA, Yeatman JD. Biological development of reading circuits. Current Opinion in Neurobiology. 2013; 23(2):261–268.

Wang K, Li X, Huang R, Ding J, Song L, Han Z. The left inferior longitudinal fasciculus supports orthographic processing: Evidence from a lesion-behavior mapping analysis. Brain and Language. 2020; 201:104721.

Wang Y, Mauer MV, Raney T, Peysakhovich B, Becker BL, Sliva DD, Gaab N. Development of tract-specific white matter pathways during early reading development in at-risk children and typical controls. Cerebral Cortex. 2017; 27(4):2469–2485.

Wassermann D, Rathi Y, Bouix S, Kubicki M, Kikinis R, Shenton M, Westin CF. White matter bundle registration and population analysis based on Gaussian processes. In: *Biennial International Conference on Information Processing in Medical Imaging* Springer; 2011. p. 320–332.

Wasserthal J, Neher P, Maier-Hein KH. TractSeg-Fast and accurate white matter tract segmentation. NeuroImage. 2018; 183:239–253.

Wasserthal J, Neher PF, Hirjak D, Maier-Hein KH. Combined tract segmentation and orientation mapping for bundle-specific tractography. Medical image analysis. 2019; 58:101559.

Wasserthal J, Neher PF, Maier-Hein KH. Tract orientation mapping for bundle-specific tractography. In: *International Conference on Medical Image Computing and Computer-Assisted Intervention* Springer; 2018. p. 36–44.

Wechsler D, Kodama H. Wechsler intelligence scale for children, vol. 1. Psychological corporation New York; 1949.

Xin W, Chan JR. Myelin plasticity: sculpting circuits in learning and memory. Nature Reviews Neuroscience. 2020; 21(12):682–694.

Yeatman JD, Dougherty RF, Ben-Shachar M, Wandell BA. Development of white matter and reading skills. Proceedings of the National Academy of Sciences. 2012; 109(44):E3045–E3053.

Yeatman JD, Dougherty RF, Rykhlevskaia E, Sherbondy AJ, Deutsch GK, Wandell BA, Ben-Shachar M. Anatomical properties of the arcuate fasciculus predict phonological and reading skills in children. Journal of cognitive neuroscience. 2011; 23(11):3304–3317.

Yeh FC, Verstynen TD, Wang Y, Fernández-Miranda JC, Tseng WYI. Deterministic diffusion fiber tracking improved by quantitative anisotropy. PloS one. 2013; 8(11):e80713.

Yeh FC, Vettel JM, Singh A, Poczos B, Grafton ST, Erickson KI, Tseng WYI, Verstynen TD. Quantifying differences and similarities in whole-brain white matter architecture using local connectome fingerprints. PLoS computational biology. 2016; 12(11):e1005203.

Yeh FC, Zaydan IM, Suski VR, Lacomis D, Richardson RM, Maroon JC, Barrios-Martinez J. Differential tractography as a track-based biomarker for neuronal injury. Neuroimage. 2019; 202:116131.

Yoo AB, Jette MA, Grondona M. Slurm: Simple linux utility for resource management. In: *Workshop on Job Scheduling Strategies for Parallel Processing* Springer; 2003. p. 44–60.

Yu X, Zuk J, Perdue MV, Ozernov-Palchik O, Raney T, Beach SD, Norton ES, Ou Y, Gabrieli JD, Gaab N. Putative protective neural mechanisms in prereaders with a family history of dyslexia who subsequently develop typical reading skills. Human brain mapping. 2020; 41(10):2827–2845.

Zhang H, Schneider T, Wheeler-Kingshott CA, Alexander DC. NODDI: practical in vivo neurite orientation dispersion and density imaging of the human brain. Neuroimage. 2012; 61(4):1000–1016.

Zhang Y, Brady M, Smith S. Segmentation of brain MR images through a hidden Markov random field model and the expectation-maximization algorithm. IEEE Transactions on Medical Imaging. 2001; 20(1):45–57. doi: 10.1109/42.906424.

Zhao C, Tapera TM, Bagautdinova J, Bourque J, Covitz S, Gur RE, Gur RC, Larsen B, Mehta K, Meisler SL, Murtha K, Muschelli J, Roalf DR, Sydnor VJ, Valcarcel AM, Shinohara RT, Cieslak M, Satterthwaite TD. ModelArray: a memory-efficient R package for statistical analysis of fixel data. bioRxiv. 2022; https://www.biorxiv.org/content/early/2022/07/14/2022.07.12.499631, doi: 10.1101/2022.07.12.499631.

Supplementary Material

Correlations Between Phenotypic and Neuroimaging Metrics

Testing for pairwise correlations between phenotypic and neuroimaging metrics of interests yielded several expected findings that validated the data collection procedures (Figure S1). These included: 1) a stronger positive link between reading skill and verbal IQ compared to the association between reading skill and visuospatial IQ; 2) an association between higher SES status and higher measures of intelligence; 3) a negative correlation between image quality and motion; 4) a strong coupling between ICV and global FC; 5) an association between better reading and larger brain volumes (***Ramus et al., 2018***); and 6) a negative association between age and motion, suggesting that older children are more compliant in the scanner. What was less expected however, was how much more variance in the global fixel metrics was captured by neighbor correlation compared to mean motion, considering that both are interpreted as image quality metrics. This may suggest that including only average motion as a covariate will not entirely control for image quality in statistical models.

Phenotypic Differences by Site

We ran one-way ANOVAs to look for site-wise differences in continuous phenotypic and neuroimaging variables. If the ANOVA was significant ($p < 0.05$), we ran *post-hoc* Tukey tests to determine the nature of these differences (Table S1; Figure S2).

Metric	*F*-statistic	CBIC vs. CUNY *t*-stat	CUNY vs. RU *t*-stat	RU vs. SI *t*-stat	CBIC vs. RU *t*-stat	CUNY vs. SI *t*-stat	CBIC vs. SI *t*-stat
Age	2.30	-	-	-	-	-	-
EHI	0.12	-	-	-	-	-	-
SES	10.67*	-	-	2.81	3.53	3.51	3.72
ICV	19.47*	-2.24	5.01	-	6.50	4.05	3.23
WISC VCI	8.06*	-	-	-	4.72	-	-
WISC VSI	9.31*	-	-	-	5.17	-	-
TOWRE	2.30	-	-	-	-	-	-
gFD	152.8*	-9.63	-	1.30	-1.97	1.04	4.30
gFC	4.04*	-	-	2.11	2.09	2.79	2.84
Motion	35.83*	-	-	-5.17	-8.11	-4.47	-7.61
Neighbor Corr.	11.59*	-5.82	5.24	-	-	2.99	-

Table S1. ANOVA results for site-wise comparisons between phenotypic and neuroimaging metrics. Group comparison columns list significant *t*-statistics. * denotes $p < 0.05$ for the ANOVA between all sites. *Post-hoc* *t*-tests were only run if the between-sites ANOVA was significant. Only significant *t*-statistics ($p < 0.05$) are shown in the table. A positive *t*-statistic denotes Site 1 > Site 2. *Abbreviations*: EHI - Edinburgh Handedness Inventory; SES - socioeconomic status; ICV - intracranial volume; TOWRE - Tests of Word Reading Efficiency composite score, age-normalized; WISC VSI - Wechsler Intelligence Scale for Children visuospatial index, age-normalized; WISC VCI - Wechsler Intelligence Scale for Children verbal comprehension index, age-normalized; gFD - globally-averaged fiber density; gFC - globally-averaged fiber cross-section.

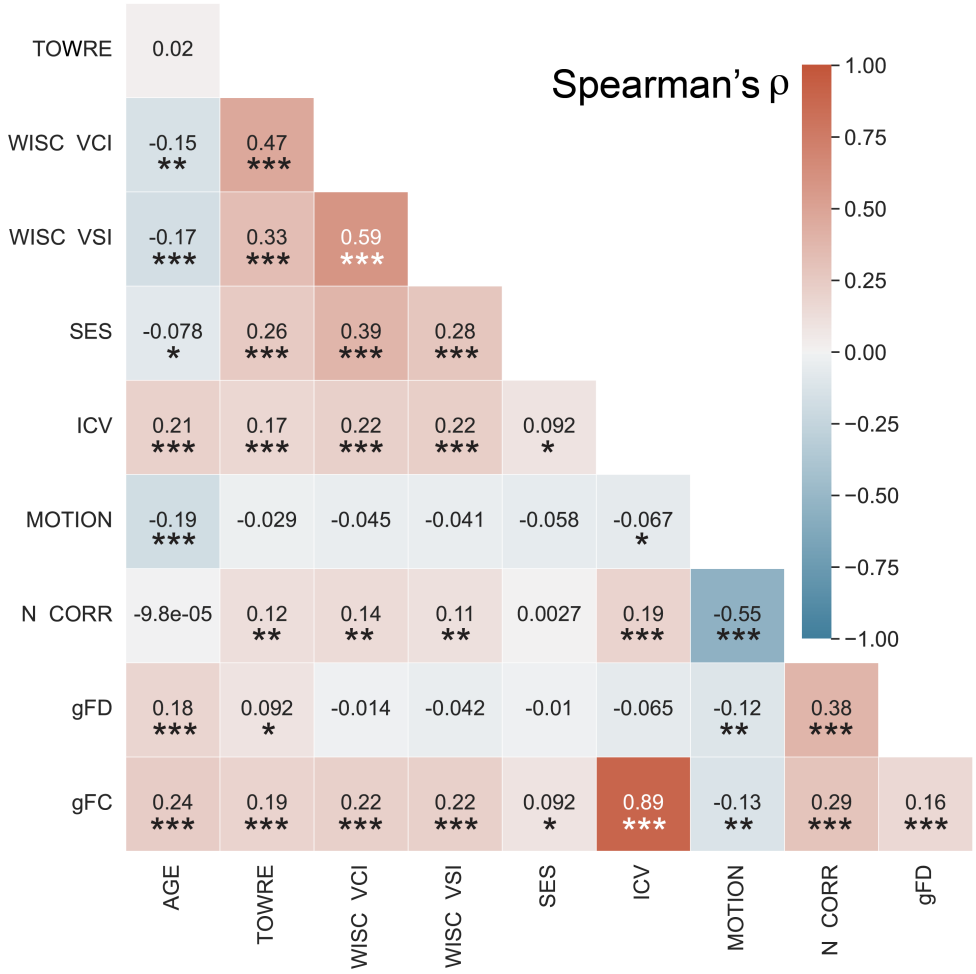

Figure S1. Correlations between continuous phenotypic and neuroimaging variables. Correlation coefficients are reported as Spearman's ρ. *p*-values were FDR Benjamini-Hochberg adjusted across tests. * - $p < 0.05$; ** - $p < 0.001$; *** - $p <$ 1e-5. *Abbreviations*: TOWRE - Tests of Word Reading Efficiency composite score, age-normalized; WISC VSI - Wechsler Intelligence Scale for Children visuospatial index, age-normalized; WISC VCI - Wechsler Intelligence Scale for Children verbal comprehension index, age-normalized; SES - socioeconomic status; ICV - intracranial volume; N Corr - neighbor correlation; gFD - globally-averaged fiber density; gFC - globally-averaged fiber cross-section.

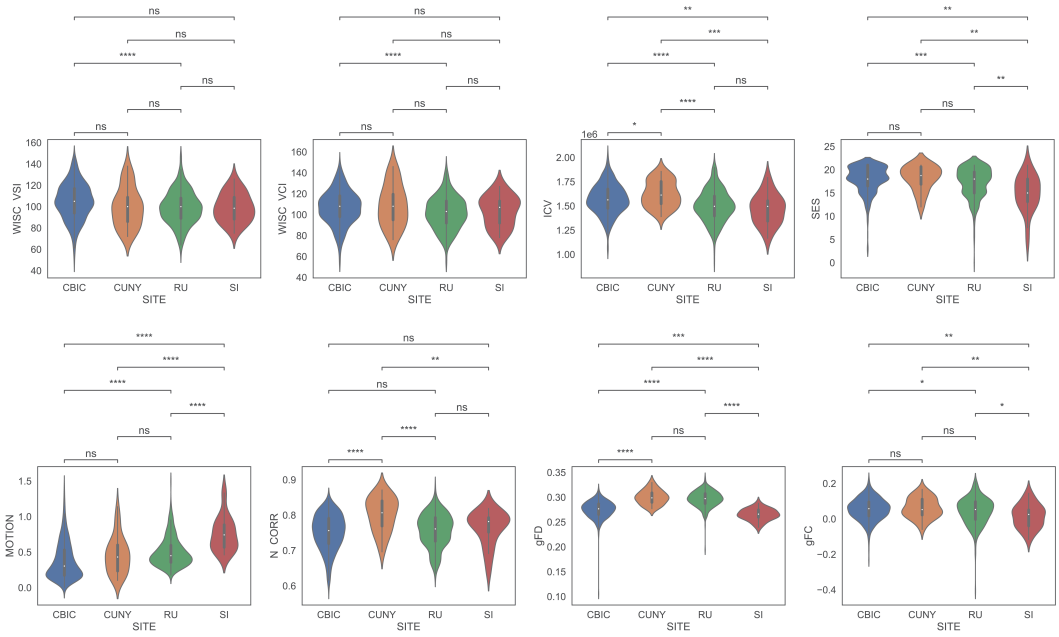

Figure S2. ANOVA results for site-wise comparisons between phenotypic and neuroimaging metrics. Only metrics associated with a significant between-sites ANOVA ($p < 0.05$) are plotted. * denotes $p < 0.05$, ** denotes $p < 0.01$, *** denotes $p <$ 1e-03, and **** denotes $p <$ 1e-04. *Abbreviations*: SES - socioeconomic status; ICV - intracranial volume; WISC VSI - Wechsler Intelligence Scale for Children visuospatial index, age-normalized; WISC VCI - Wechsler Intelligence Scale for Children verbal comprehension index, age-normalized; N Corr - neighbor correlation; gFD - globally-averaged fiber density; gFC - globally-averaged fiber cross-section.

FBA Additional Figures and Secondary Analyses

We note that exploratory fixel-based analyses reported in the supplementary materials are not corrected for multiple-comparisons.

DTI, DKI, and NODDI Correlation Analyses

We used *QSIPrep* version 0.15.3 to run the `dipy_dki` (***Henriques et al., 2021***) and `amico_noddi` (***Daducci et al., 2015***) reconstruction pipelines on the preprocessed data. From the `dipy_dki` pipeline, we collected fractional anisotropy (FA), mean diffusivity (MD), kurtosis fractional anisotropy (KFA), and mean kurtosis (MK). From `amico_noddi`, we collected the neurite density index (NDI - synonymous with intracellular volume fraction or ICVF) and orientation dispersion index (ODI). We resampled and warped these scalar maps to the 1.25mm isotropic template space, and then mapped the voxel values to fixels. While each fixel in a voxel is initially assigned the same value, spatial smoothing is still applied on the fiber population level. We then used *ModelArray* to run models relating each of these metrics to the composite age-standardized TOWRE scores. Similar to the primary analyses of FDC, model confounds included a spline fit for age and linear fits for sex, site, quality (neighbor correlation), and log(ICV). The only metric that yielded significant findings was ODI, which was inversely related to reading skills in bilateral temporoparietal and cerebellar regions (Figure S7). The peak effect size (ΔR^2_{adj}) achieved was 0.023.

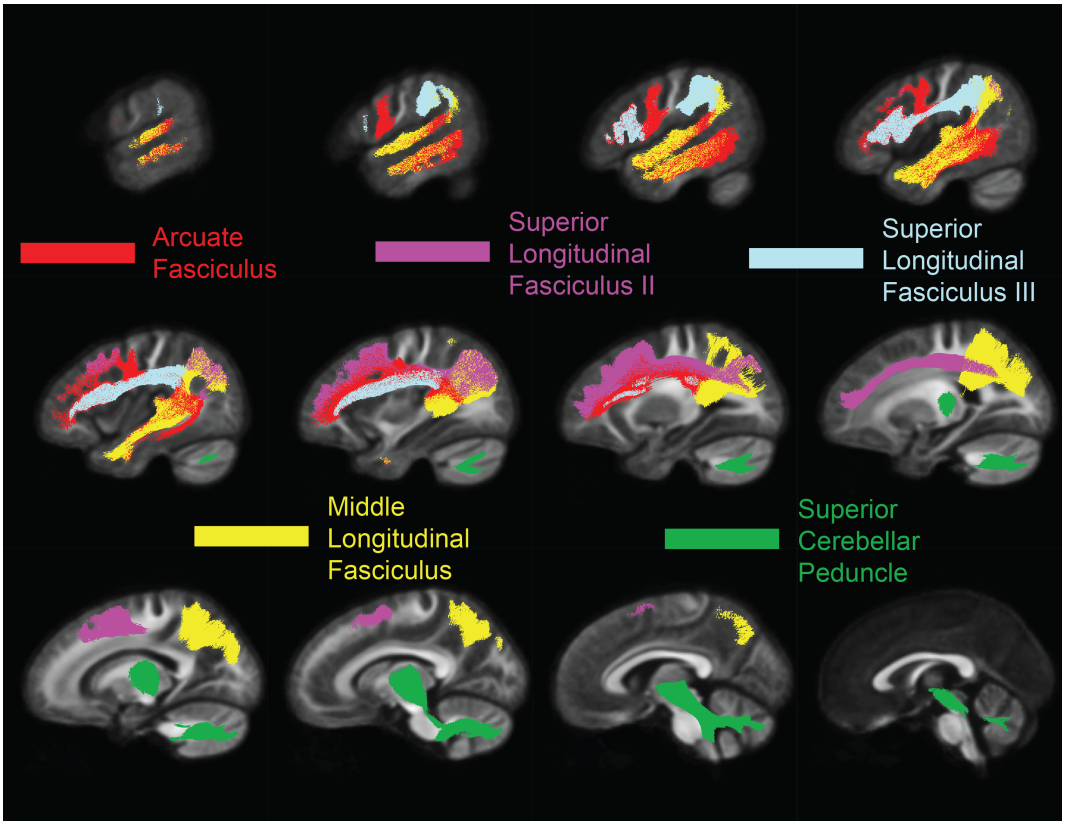

Figure S3. Plots of the set of tracts in which the strongest effect sizes ($\Delta R^2_{adj} > 0.03$) were achieved for relating FDC to TOWRE scores. All tracts were in the left hemisphere. Sagittal slices go from lateral-to-medial. Tracts were segmented from and are plotted on top of the FOD template.

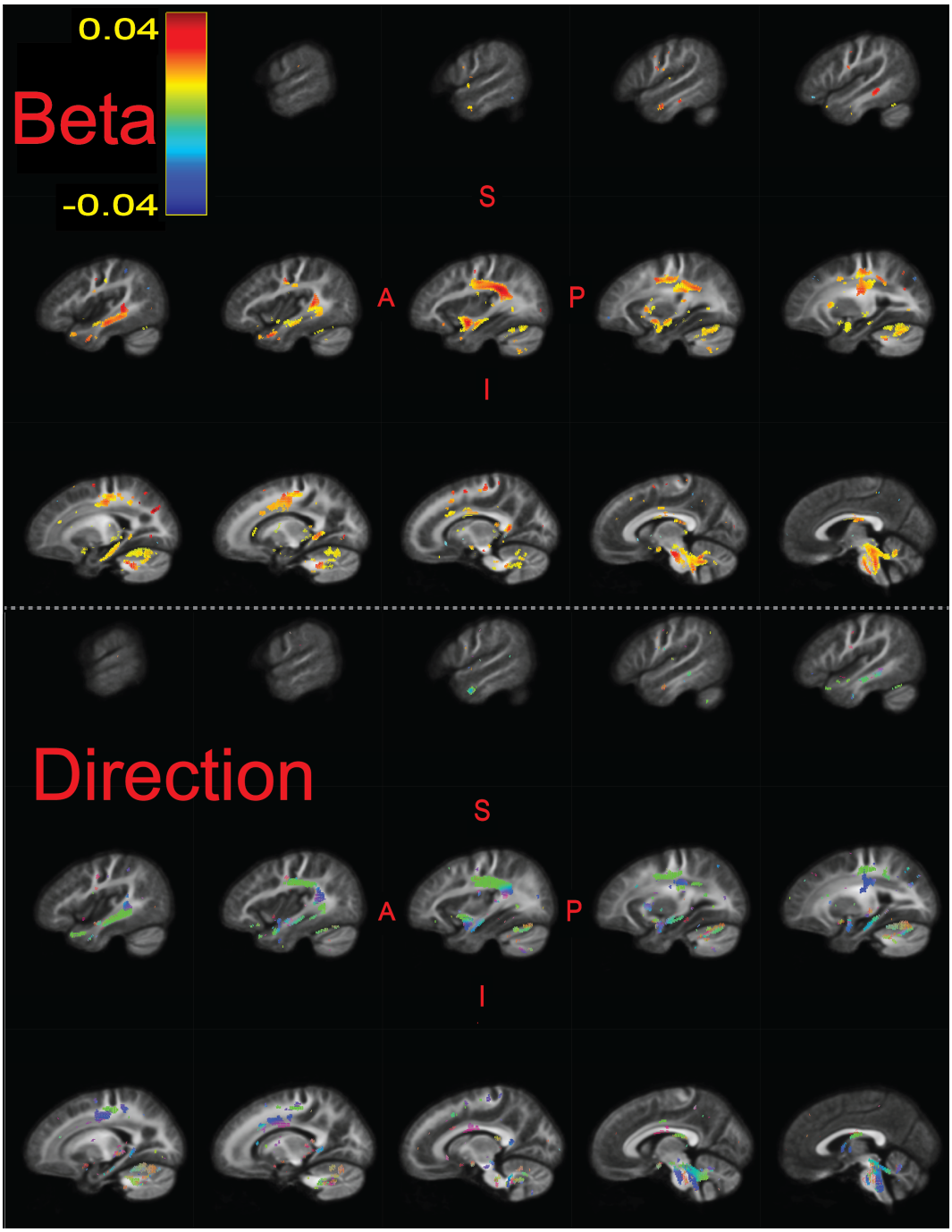

Figure S4. Significant fixels ($q_{FDR} < 0.05$) relating FDC to TOWRE scores, colored by the beta estimates (top) and direction (bottom; Red - LR, Green - AP, Blue - SI). Model confounds included a spline fit for age and linear fits for sex, site, neighbor correlation, and log(ICV). Only the left hemisphere is shown. Sagittal slices go from lateral-to-medial. The template FOD image was used as the background image.

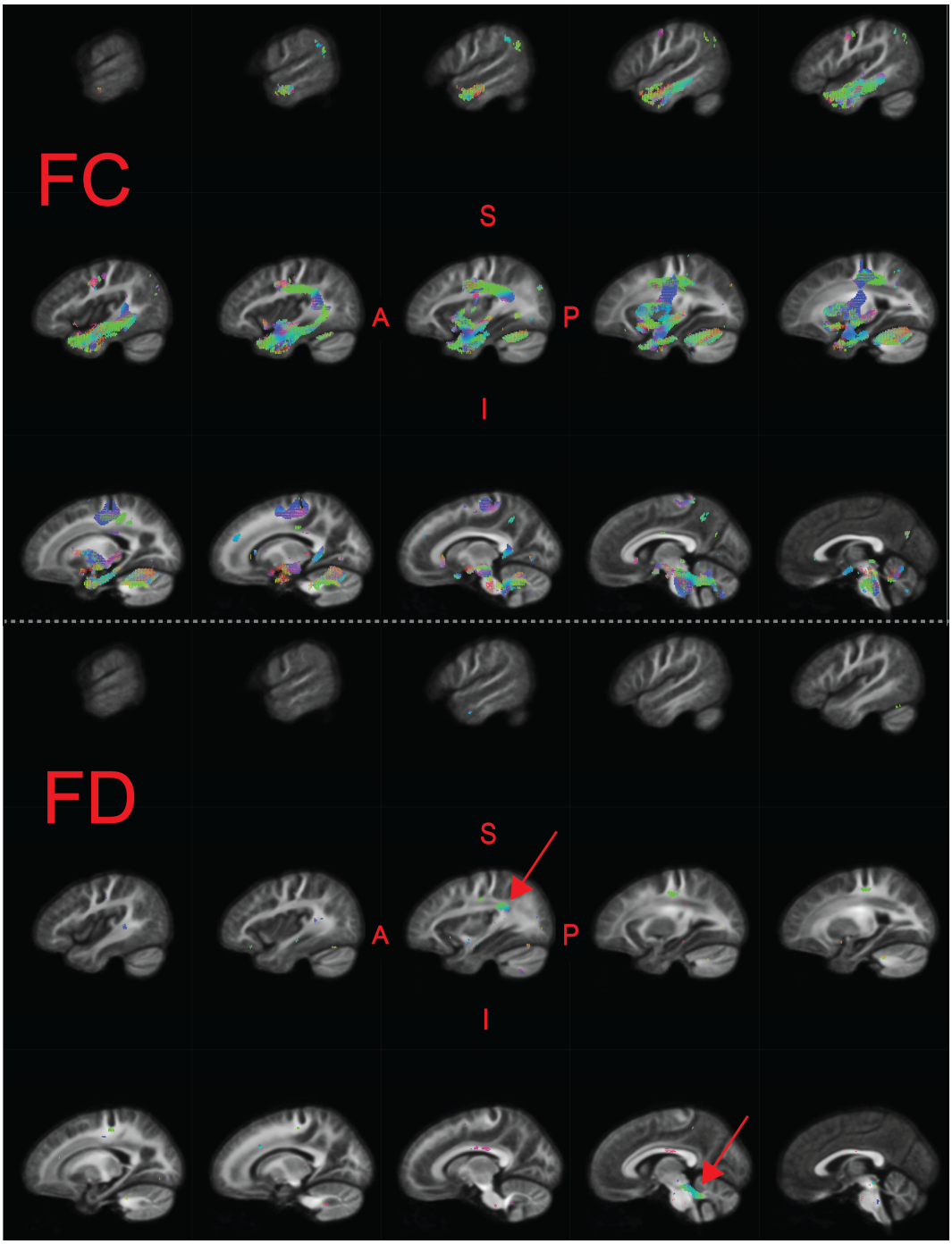

Figure S5. Significant fixels ($q_{FDR} < 0.05$) relating fiber cross-section (FC; top), and fiber density (FD; bottom) to TOWRE scores, colored by direction (Red - LR, Green - AP, Blue - SI). Model confounds included a spline fit for age and linear fits for sex, site, and neighbor correlation. Additionally, FC included an additional regressor for log(ICV). Only the left hemisphere is shown. Sagittal slices go from lateral-to-medial. Red arrows point to larger clusters of significant fixels in temporoparietal and cerebellar white matter that overlapped with significant results in the main FDC analysis. The template FOD image was used as the background image.

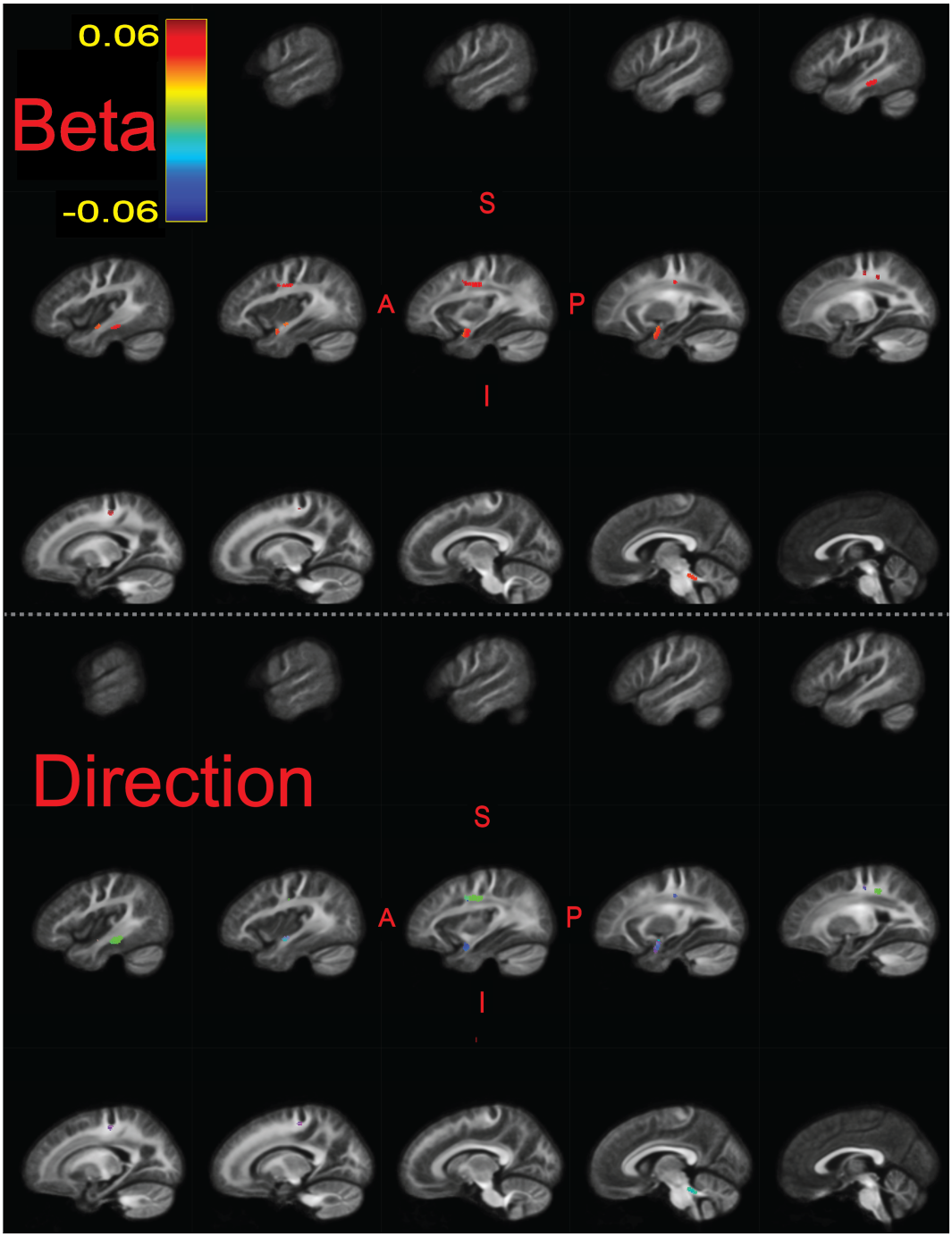

Figure S6. Significant fixels ($q_{FDR} < 0.05$) for group differences in fiber cross-section between the TR and RD groups. The top panel is colored be beta coefficients (positive indicates TR > RD), and bottom panel is colored by direction (Red - LR, Green - AP, Blue - SI). Model confounds included a spline fit for age and linear fits for sex, site, neighbor correlation, and log(ICV). Only the left hemisphere is shown. Sagittal slices go from lateral-to-medial. The template FOD image was used as the background image.

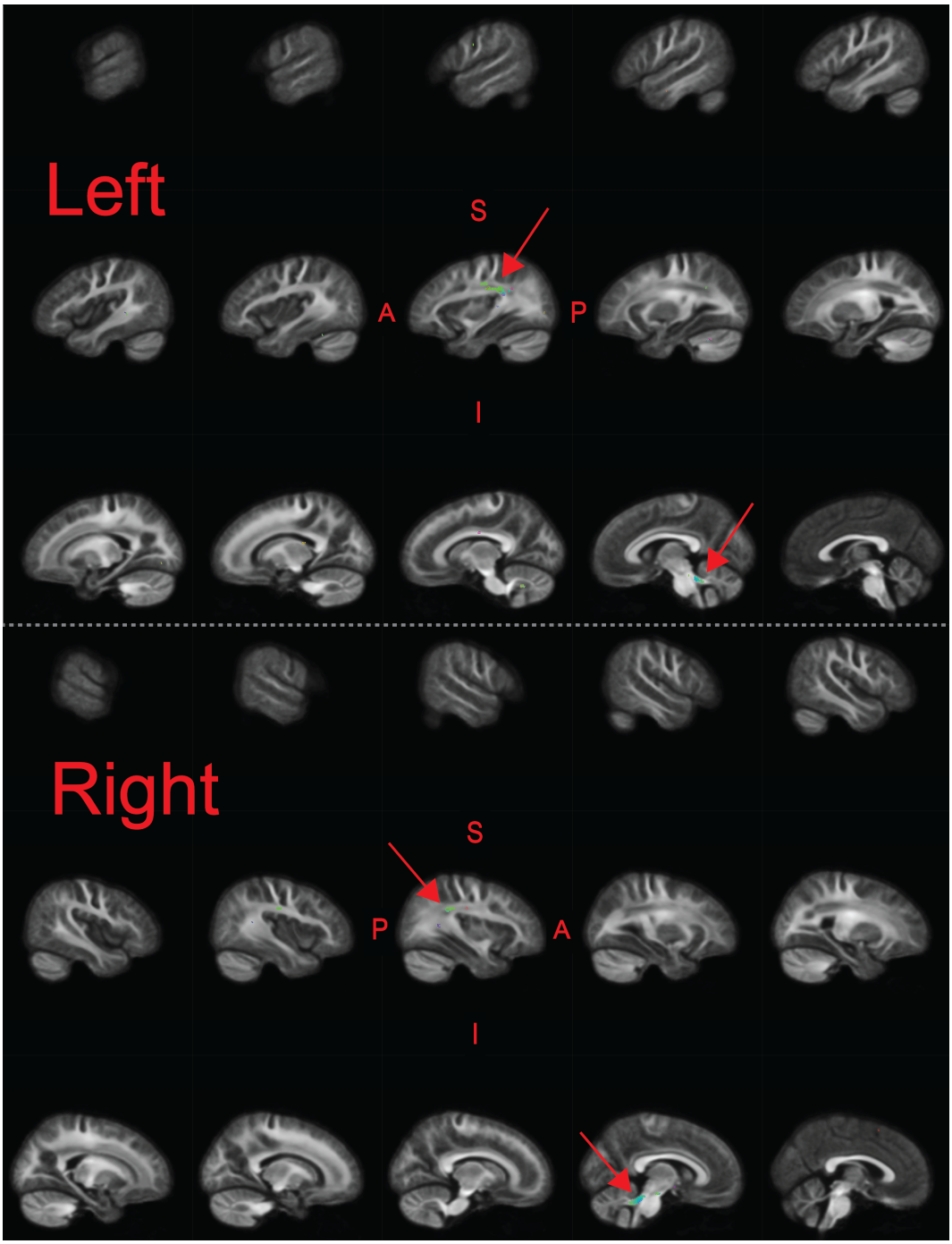

Figure S7. Significant fixels ($q_{FDR} < 0.05$) relating orientation dispersion index (ODI) to TOWRE scores, colored by direction (Red - LR, Green - AP, Blue - SI). Model confounds included a spline fit for age and linear fits for sex, site, neighbor correlation, and log(ICV). Top and bottom panels are left and right hemispheres, respectively. Sagittal slices go from lateral-to-medial. Red arrows point to larger clusters of significant fixels in bilateral temporoparietal and cerebellar white matter. The template FOD image was used as the background image.